Identification of the drug/metabolite transporter 1 as a marker of quinine resistance in a NF54×Cam3.II *P. falciparum* genetic cross.

Mariko Kanai[1,2], Sachel Mok[1-3], Tomas Yeo[1,2†], Melanie J. Shears[4†], Leila S. Ross[1], Jin H. Jeon[1,2], Sunil Narwal[1,2], Meseret T. Haile[1], Abhai K. Tripathi[4], Godfree Mlambo[4], Jonathan Kim[5], Eva Gil-Iturbe[6], John Okombo[1,2], Kate J. Fairhurst[1,2], Talia Bloxham[1,2], Jessica L. Bridgford[1,2], Tanaya Sheth[1,2], Kurt E. Ward[1,2], Heekuk Park[3], Felix D. Rozenberg[3], Matthias Quick[5-7], Filippo Mancia[5], Marcus C.S. Lee[8,9], Jennifer L. Small-Saunders[1-3], Anne-Catrin Uhlemann[2,3], Photini Sinnis[4], David A. Fidock[1-3*]

[1]Department of Microbiology & Immunology, Columbia University Irving Medical Center, NY, USA; [2]Center for Malaria Therapeutics and Antimicrobial Resistance, Columbia University Irving Medical Center, NY, USA; [3]Division of Infectious Diseases, Department of Medicine, Columbia University Irving Medical Center, NY, USA; [4]Department of Molecular Microbiology and Immunology, Johns Hopkins Bloomberg School of Public Health, MD, USA; [5]Department of Physiology and Cellular Biophysics, Columbia University Irving Medical Center, NY, USA; [6]Department of Psychiatry, Columbia University Irving Medical Center, NY, USA; [7]Division of Molecular Therapeutics, New York State Psychiatric Institute, NY, USA; [8]Wellcome Sanger Institute, Wellcome Genome Campus, Hinxton, UK; [9]Biological Chemistry and Drug Discovery, Wellcome Centre for Anti-Infectives Research, University of Dundee, Dundee, UK.

[†]These authors contributed equally to this work.
*Corresponding author's email address: df2260@cumc.columbia.edu

Abstract

The genetic basis of *Plasmodium falciparum* resistance to quinine (QN), a drug used to treat severe malaria, has long been enigmatic. To gain further insight, we used FRG-NOD human liver-chimeric mice to conduct a *P. falciparum* genetic cross between QN-sensitive and QN-resistant parasites, which also differ in their susceptibility to chloroquine (CQ). By applying different selective conditions to progeny pools prior to cloning, we recovered 120 unique recombinant progeny. These progeny were subjected to drug profiling and QTL analyses with QN, CQ, and monodesethyl-CQ (md-CQ, the active metabolite of CQ), which revealed predominant peaks on chromosomes 7 and 12, consistent with a multifactorial mechanism of resistance. A shared chromosome 12 region mapped to resistance to all three antimalarials and was preferentially co-inherited with *pfcrt*. We identified an ATP-dependent zinc metalloprotease (FtsH1) as one of the top candidates and observed using CRISPR/Cas9 SNP-edited lines that *ftsh1* is a potential mediator of QN resistance and a modulator of md-CQ resistance. As expected, CQ and md-CQ resistance mapped to a chromosome 7 region harboring *pfcrt*. However, for QN, high-grade resistance mapped to a chromosome 7 peak centered 295kb downstream of *pfcrt*. We identified the drug/metabolite transporter 1 (DMT1) as the top candidate due to its structural similarity to PfCRT and proximity to the peak. Deleting DMT1 in QN-resistant Cam3.II parasites significantly sensitized the parasite to QN but not to the other drugs tested, suggesting that DMT1 mediates QN response specifically. We localized DMT1 to structures associated with vesicular trafficking, as well as the parasitophorous vacuolar membrane, lipid bodies, and the digestive vacuole. We also observed that mutant DMT1 transports more QN than the wild-type isoform *in vitro*. Our study demonstrates that DMT1 is a novel marker of QN resistance and a new chromosome 12 locus associates with CQ and QN response, with *ftsh1* is a potential candidate, suggesting these genes should be genotyped in surveillance and clinical settings.

Introduction

In the year 2022, there were an estimated 249 million malaria cases in 85 malaria endemic countries, and an estimated 619,000 deaths, a majority of which were in African children[1]. The current first-line chemotherapies for *Plasmodium falciparum* uncomplicated malaria are artemisinin-based combination therapies (ACTs), which combine fast-acting yet rapidly cleared artemisinin (ART) derivatives with longer-lasting partner drugs. For severe malaria, the first-line treatment is artesunate, which can be replaced by artemether or by quinine (QN) when these ART derivatives are not available or are contraindicated. However, *Plasmodium falciparum* resistance to antimalarial drugs remains a threat to malaria elimination efforts.

Alarmingly, mutant *k13*-mediated ART-resistant *P. falciparum* parasites have become widespread in Southeast Asia[2], and have recently emerged independently in Uganda, Rwanda, and Eritrea[3]. In preparation for the possibility of widespread *P. falciparum* resistance to ARTs in Africa and consequent loss of ART and ACT efficacy, alternative drugs with distinct modes of action are urgently needed. Despite the progress made in developing several promising preclinical candidates, many challenges remain and their implementation in the field is years away. Alternative approaches currently being considered for this inevitable gap in treatment options are to add a third, existing drug to ACTs (hence called triple ACTs) and to reintroduce drugs such as QN, as was done after the prior failure of chloroquine (CQ). QN is of particular interest as it has retained efficacy since its first use in the 1600s[4] as resistance has been slow to develop. The first report of QN resistance was in ~1910 in Brazil[5,6], with more recent evidence from the Ivory Coast[7], Nigeria[8], French Guiana[9-11], Thailand[12], Senegal[13], Laos[14], Cameroon[15], Uganda[16], and Gabon[17]. In these cases, resistance to QN was usually low-grade, with QN having a delayed or reduced effect. Reported instances of QN treatment failure may also be attributed to reasons other than parasite resistance, including variability in QN pharmacokinetics as well as QN drug quality and compliance (due to its seven-day course).

Given the current clinical use of QN as well as the potential for its increased future use, it is critical to gain a better understanding of QN mechanism of resistance. This is thought to be multifactorial and has been partially associated with polymorphisms in *pfcrt* (via single nucleotide polymorphisms (SNPs)), *pfmdr1* (both copy number and SNPs), *pfnhe-1* (DNNND repeat polymorphisms)[18], and the HECT E3 ubiquitin ligase *pfut* (SNPs)[19]. The minor suspected contributions of *pfnhe-1* and *pfut* to QN resistance appear to be restricted to certain strains, suggesting the involvement of other genetic loci[19,20]. QN, mefloquine, and lumefantrine are all classified as aryl-amino alcohols (Extended Data 1a) and have been suggested to share resistance mechanisms although the exact mechanisms remain unclear[21-24].

Chloroquine (CQ) is a 4-aminoquinoline (Extended Data 1a) and former first-line drug for *P. falciparum* (that is still in use for *P. vivax*), and it's replacement with artemether-lumefantrine has been associated with the recent emergence of CQ-sensitive *P. falciparum* parasites[25,26]. CQ is known to act on the heme detoxification pathway by diffusing into the acidic digestive vacuole, where it is protonated and binds to heme,

preventing its detoxification into hemozoin and eventually the heme buildup kills the parasite; the *P. falciparum* chloroquine resistance transporter (PfCRT) has been identified as the primary determinant of parasite resistance to CQ and single-nucleotide polymorphisms (SNPs) in PfCRT were experimentally shown to confer resistance to CQ[27]. No secondary modulator of CQ resistance has been identified aside from a small contribution from another DV membrane transporter PfMDR1 (notably its N86Y variant) on a PfCRT-mutant background[28-32].

Of note, CQ and QN responses have often been divergent[33,34] (indicative of non-*pfcrt* and non-*pfmdr1* mediators of QN resistance), whereas MFQ and QN responses have often been similar. The parasite genetic background appears to play a role in these responses. The QN mode of action has been partially associated with heme detoxification but remains enigmatic. In a recent study, when *P. falciparum* parasites were pressured with artesunate in a humanized mouse model, parasites that were highly ART-resistant (10× fold increase) and moderately QN-resistant (4×) emerged and no mutations were found in *k13* or *pfnhe-1*, but PfMDR1 had amplified to two copies and acquired the N86Y mutation[35].

Genetic crosses are a powerful forward genetics tool to investigate the molecular basis of a variety of phenotypes, including drug resistance. Analyses of cross progeny have identified mutations in *dhps* as determinants of *P. falciparum* resistance to sulfadoxine[36], *dhfr* for resistance to pyrimethamine[37], *pfcrt* for resistance to CQ[38-40], and have also been applied to study non-*k13* mediated ART resistance mechanisms[28,41,42]. Earlier *P. falciparum* genetic crosses utilized splenectomized chimpanzees to complete the human stages of the *Plasmodium* life cycle[43-46]. However, their application to biomedical research has been banned, prompting the development of a protocol[47] that uses FRG-NOD human liver-chimeric (huHep) mice[48], which has now been used for several recent crosses[41,42,47]. To explore the genes underlying *P. falciparum* resistance to QN and CQ, we conducted a genetic cross between a Cambodian (Cam3.II) and African (NF54) parasites that differ in their susceptibility to these drugs.

Results

QN partially inhibits heme detoxification

The 4-aminoquinolines CQ and ADQ are known to inhibit the detoxification of toxic heme moieties by preventing their incorporation into chemically inert Hz. This occurs in the DV, particularly during the trophozoite stage of intra-erythrocytic parasites[49,50]. To explore this mechanistic aspect of drug action, we tested whether QN and MFQ also inhibit the heme detoxification pathway. We employed a detergent-based β-hematin assay[51-53], in which a hydrophobic, nonionic, lipophilic detergent, Nonidet P-40 (NP-40), is used to mimic the neutral lipid droplets at the site of crystal formation in the DV and promote the mineralization of hematin (a dimeric form of heme) into synthetic hemozoin (β-hematin) formation *in vitro*. After incubation of compounds with hematin, we quantified the amount of unconverted hematin using the pyridine ferrihemochrome method, which relies on aqueous pyridine specifically forming a low-spin complex with hematin but not β-hematin and the complex having an absorbance at 405nm. In these assays, the IC_{50} refers to the drug concentration that inhibits hemozoin formation by 50%. We found that QN (mean

IC_{50}±SEM = 22.1±1.2 μM) and MFQ (mean IC_{50}±SEM = 33.8±4.6 μM) inhibited β-hematin formation to a lesser degree than the known hemozoin formation inhibitors, CQ (mean IC_{50}±SEM = 11.2±0.5 μM) and md-ADQ (mean IC_{50}±SEM = 5.2±1.0 μM). QN was a more potent hemozoin inhibitor than MFQ. These results are consistent with the structural similarity of QN and MFQ as quantified by Tanimoto scores (*T*) in Table S13, and previous reports showing potential partial involvement of QN and MFQ in the heme detoxification pathway[54]. Representative biological replicate dose-response curves for these drugs, together with the negative control compounds pyrimethamine (antifolate), doxycycline (protein synthesis inhibitor), and DMSO, are shown in Extended Data 1b. Mean±SEM IC_{50} values for these drugs (as well as AS) are shown in Table S14. Those negative control inhibitors had IC_{50} values >500 μM.

A novel NF54×Cam3.II *P. falciparum* genetic cross was conducted using human liver-chimeric mice

To identify genetic determinants of antimalarial drug resistance, we implemented a genetic cross between the NF54 and Cam3.II parasites. The NF54 JHU (shortened hereafter as NF54) parasite strain was isolated in 1979 in the Netherlands and based on its genome sequence is postulated to be of African origin[55]. The Cam3.II G8 (shortened hereafter as Cam3.II) parasite is a clone of the previously reported[56,57] Cam3.II clinical isolate (also known as RF967 or PH0306-C) that was isolated in western Cambodia.

These two parasites selected based on their genetic and phenotypic differences, as Cam3.II is multidrug resistant and has mutant alleles in known drug resistance mediators, while NF54 is sensitive to common and first-line antimalarials and has the WT reference sequence, enabling the investigation of resistance mechanisms to multiple antimalarial drugs (Fig. 1a). Of note, Cam3.II is resistant to CQ and moderately resistant to QN. Cam3.II harbors the mutant Dd2 isoform of *pfcrt* that is the major determinant of CQ resistance, as well as genetic variants that have been partially associated with QN resistance (*pfut*: P535L / T589S / R735K / Y1232C / *N1375S* / P1384A / *Y1387F* / D1419N / D1864N / E2355A / K2659N; the italicized SNPs were associated with QN resistance[19], along with *pfcrt* and *pfmdr1*. In contrast, NF54 is sensitive to both drugs and has the WT alleles for these genes, indicating the high potential for identifying QN resistance mediators and CQ secondary resistance modulators from these genetically and phenotypically distinct parents.

To perform the genetic cross, we mixed mature gametocytes from the NF54 and Cam3.II parasites at a 1:1 ratio (0.3% gametocytemia each) and fed them to 4–6-day old female *Anopheles stephensi* mosquitoes (Liston strain) using glass membrane feeders (Extended Data 2a). The parental gametocytes convert into gametes upon transmission and then fuse in the mosquito midgut, where sexual reproduction and recombination occurs (if gametes from distinct parents mate) during the subsequent brief diploid zygote stage. The resulting meiotic products develop into motile ookinetes and then later oocysts, which undergo sporogony and mitotic division that produces thousands of haploid sporozoites from each oocyst[58]. The oocyst prevalence was ~20 oocysts per mosquito midgut and ~40,000 sporozoites were counted per mosquito (Table S1). We infected four FRG NOD human liver-chimeric (huHep) with ~200,000–240,000 progeny

sporozoites by natural mosquito bite or intravenous (IV) inoculation. After the progeny underwent the human liver and blood stages in the humanized mice, we recovered haploid asexual blood-stage (ABS) parasites seven days post-infection and cultured them *in vitro* for one–two cycles before cryopreservation.

Recovery of 120 unique recombinant progeny following the application of differing selective conditions to bulk progeny pools

Initially, we thawed progeny bulk freezes from four mice (A–D), expanded these cultures under no drug pressure (referred to herein as 'no drug bulks') and cloned the progeny by limiting dilution (Extended Data 2b). We conducted PCR and gel electrophoresis-based Microsatellite (MS) genotyping of gDNA from these progeny using the 11 markers listed in Table S3, which detected non-parental recombinant progeny. This work yielded 162 clonal progeny (listed in Tables S2 and S4), of which 71 were chosen for WGS analysis. To obtain additional unique recombinants, we also subjected bulk progeny pools from mice B and C to various CQ and QN drug pressures (Extended Data 2c, Table S2). We applied CQ 50nM, CQ 75nM, QN 75nM, QN 95nM for 3 days, while we applied QN 140nM (and later 240nM), and QN 180nM for 4 days on the 'no drug' bulks or the QN 95nM-pre-pressured bulks. After a drug wash-off and a recovery period, we obtained 133 clonal progeny from CQ pressure and an additional 292 from QN pressure. We conducted multiplexed PCR and fragment analysis-based MS genotyping (Table S3) as well as SNP PCR and Sanger sequencing genotyping on the progeny obtained after CQ and QN 75nM and 95nM pressure to screen for clonal recombinants and performed WGS on a subset of 92 clonal progeny. As the primary goal of the higher concentration QN selections was to recover QN-resistant progeny, we split cloning plates 1:2 for progeny obtained after QN 140nM, 180nM, and 140+240nM and subjected plates to 72 hr of QN 140nM pressure, with surviving resistant parasites then proceeding to WGS analysis for a set of 95 progeny. PCR and fragment analysis as well as PCR and gel electrophoresis-based MS genotyping always correctly predicted the self-fertilized or recombinant status of the progeny, which was also confirmed by WGS.

For each progeny, we classified alleles at each of the 13,116 SNP positions (described in Table S5) based on WGS data that distinguish NF54 from Cam3.II. Hierarchical clustering was then used to identify isogenic progeny and assign haplotypes. In total, the recombinant progeny segregated into 120 haplotypes (for a set of 122 total when including the parental strains; Table S7). The haplotypes were also clustered by the selection pressure applied before cloning (Fig. 1b). 55 unique recombinant haplotypes were obtained after no drug pressure prior to cloning, while CQ and QN pressure yielded an additional 65 distinct recombinant haplotypes. As we obtained isogenic recombinant progeny after more than one selective pressure, we also examined the origins of each haplotype. 101 out of 120 unique recombinant haplotypes (84.2%) originated from only one condition (no drug, QN 75nM, QN 95nM, CQ 50nM, or CQ 75nM), suggesting there is a benefit to applying different drug concentrations of the same drug. The higher-grade QN selection pressures (QN 140nM, 180nM, 240nM) yielded nine haplotypes, which were not observed after no drug pressure, suggesting that high-grade selection can help to recover rare recombinants (and potentially those with a fitness cost), but at the cost of recovering a diverse set of progeny. In addition, only 5 of the 120 unique recombinant

haplotypes were represented by progeny obtained after both CQ and QN selection, suggesting that mechanisms of resistance to these drugs are mostly distinct.

We examined allele frequency skews in each progeny haplotype by calculating the % frequency for NF54 and Cam3.II alleles across the 13,116 SNP positions (Extended Data 3, Table S7). Most haplotypes did not show any major skews that deviated from the expected ~40–60% allele frequencies, with only Haplotype (H) 004 (from no drug), H079 (CQ 75nM and QN (95nM+140nM)), and H111 (QN 95nM) showing >70% Cam3.II allele frequency. We also calculated the *pfcrt*-specific allele frequencies in unique recombinant haplotypes obtained within each drug selection condition (Supplemental Fig. 1a), meaning some haplotypes were represented in more than group in the bar chart. As expected, all CQ-selected progeny possessed mutant Dd2 *pfcrt*, thus validating our CQ selection conditions. Despite the progeny bulk pools being cultured in serum and and the Cam3.II QN IC_{50} being 92nM in serum, a majority of the QN 95nM (~1× IC_{50}) pressured progeny had WT *pfcrt*, which was also observed in the QN (95nM+140nM) (1× and 1.5× IC_{50}) and the QN (95nM+180nM) (1× and 2× IC_{50}) selection conditions. These findings corroborate previous literature that *pfcrt* is not the primary determinant of QN resistance.

As the apicoplast and mitochondria are maternally co-inherited (and non-recombining) in *P. falciparum*[59-61], we also examined the SNPs in these genomes to classify haplotypes as having NF54 or Cam3.II maternal apicoplast and mitochondrial co-inheritance (Table S7). We note that all progeny belonging to a specific haplotype shared the same mitochondrial and apicoplast alleles, implying that they likely all originated from an identical meiotic event. We also noted a trend of CQ 75nM and the QN 140nM, QN 180nM and QN 240nM skewing towards Cam3.II maternal inheritance, although the low numbers of haplotypes recovered from some selections prevented a more definitive assessment. No other major skews were observed in the other six selection conditions. This lack of skew was interesting, as ~7× more NF54 selfed progeny were obtained compared to the Cam3.II selfed progeny after no drug pressure (Supplemental Fig. 1c, Table S4). This observation suggests that the overrepresentation of the NF54 selfed progeny after 'no drug' cloning was most likely not due to a defect in the Cam3.II gametocytogenesis of either sex, unlike the Dd2 male gametocytogenesis defect earlier observed in the HB3×Dd2 cross in which Dd2 always served as the female parent[62]. Instead, the bias towards NF54 selfing was likely due to enhanced transmissibility of NF54 as we found higher *in vitro* gametocyte counts in NF54 parasites relative to Cam3.II after gametocytogenesis induction via media stress (data not shown). In a previous HB3×3D7 genetic cross[63], nearly all apicoplast and mitochondrial genomes were inherited from the 3D7 female parent; however, biparental inheritance was also observed in two recent genetic crosses[64].

Bulk segregant analysis of *P. falciparum* resistance to quinine identifies overlapping QTLs on chromosome 7

We harvested gDNA of the bulk progeny pools after the 4-day QN 140nM, 180nM, or 240nM selection and recovery period (expanding to ~2% parasitemia), within days of establishing parasite cloning plates (Extended Data 2b,c). We also collected two 'no drug' controls for each selection. The 'D0' control gDNA was harvested at the start ('D0') of

every QN pressure. Also, before the QN selection, the starting progeny bulk pool was split into two, and one was kept on 'no drug' media and had its gDNA harvested at the same time as the post-QN selection gDNA ('no drug timepoint' control gDNA). We harvested a total of 33 bulk pool gDNA samples and obtained their WGSs (Table S9).

For bulk segregant analysis, we compared "high bulk" and "low bulk" (e.g. QN selection vs 'no drug timepoint control, QN selection vs D0 control, or 'no drug timepoint control' vs D0 control). We calculated the genome-wide Δ(SNP-*index*) and G' statistic values of the individual SNPs with a window size of 100,000 bp using QTLseqr[65] to identify the statistical significance of QTL analysis. Significance was classified as False Discovery Rate $<$0.01 or Confidence Interval (CI) $>$99% or 95%, respectively. Two pairwise comparisons between QN selection and their 'D0' controls yielded largely consistent QTLs: B: QN95 nM D0 vs B (QN95 + 180nM) and B: QN95 nM D0 vs B (QN95 + 140nM) (Extended Data 4). As expected, the comparison with the higher QN concentration (180nM) yielded higher G' values and a significant chromosome 7 peak with False Discovery Rate $<$0.14 that was driven by the QN-resistant Cam3.II alleles (Table S10). Although this 58kb region did not contain any known drug resistance markers, it was 33kb upstream of *dmt1*, a gene that will be described shortly.

While bulk segregant analysis of ART resistance[41], for example, was able to detect a single significant QTL on chr 13 containing its known primary driver of resistance, *k13*, QN bulk segregant analysis proved to be more difficult as many QTLs were detected and were not necessarily consistent across different selection conditions. This different result can most likely be attributed to QN resistance being a multigenic trait and lacking a strong primary driver. However, applying different QN selective pressures helped us to identify common QTL on chromosome 7, highlighting how bulk segregant analysis can still be used as a screening tool for multigenic traits to identify regions of interest. Bulk segregant analysis, however, needs to be followed-up by progeny clone-based QTL analysis to narrow down candidate genes and reveal epistatic relationships.

Progeny clone-based trait mapping identifies a non-*pfcrt* chr 7 locus for high-grade quinine resistance, and a novel chr 12 peak for quinine, chloroquine, and md-chloroquine

We assessed the recombinant ring-stage progeny susceptibility to CQ (N=52), its active metabolite md-CQ (N=82), and QN (N=92) by conducting 72-hour *in vitro* dose-response assays with serially diluted CQ, md-CQ, and QN. These assays allowed us to determine the half-maximal growth inhibition concentration relative to the no drug control (IC_{50}), as well as concentration to inhibit 90% of growth (IC_{90}), a metric of high-grade resistance, for these drugs (Fig. 1c-e, Extended Data 5a). Using the IC_{50} and IC_{90} values as "phenotypes" and their WGSs as "genotypes," we conducted progeny clone-based QTL analyses (Fig. 2, Extended Data 5b,c). Significant QTL segments are listed in Fig. 2e, and the genes within these segments are shown in Table S8.

For md-CQ and CQ, we only found two shared major peaks—a chromosome 7 peak harboring *pfcrt* and a novel chromosome 12 peak that appears to be usually co-inherited with *pfcrt* (Fig. 2c,e, Extended Data 5). This chromosome 12 QTL segment has not been

previously associated with CQ response, to our knowledge. A prior linkage analysis study examining CQ response (at the IC_{90} level) using the HB3×Dd2 progeny identified a single QTL on chromosome 7 containing the CQ-resistant Dd2 *pfcrt* allele that accounted for >95% of variation in CQ response[18].The md-CQ IC_{90} and CQ IC_{50} and IC_{90} chromosome 12 peak consists of 30 genes, of which 10 genes have nonsynonymous SNPs between the parents that are also found in field populations (Table S8). An additional significant but smaller peak was observed for md-CQ.

For the QN QTL analysis, statistically significant peaks were obtained on chromosomes 6, 7 and 12, and several other minor QTLs with lower LOD scores, confirming that QN resistance is multigenic (Fig. 2a,b,d). The chromosome 12 QTL for QN IC_{50} level response encompassed the CQ and md-CQ QTL, while the QN IC_{90} level chromosome 12 QTL perfectly matched the CQ and md-CQ IC_{90} segments. Excitingly, while the QN IC_{50} chromosome 7 peak centered close to *pfcrt*, the QN IC_{90} (high-grade resistance) peak was centered 296kb from *pfcrt* and encompassed 33 genes with nonsynonymous SNPs between the cross parents (Fig. 2e, Table S8).

samc, _thzk_, and _ftsh1_ as candidates driving the chr 12 md-CQ, CQ, and QN QTLs

Of the 30 genes within the md-CQ IC_{90}, QN IC_{90}, and CQ chr 12 QTL loci, and excluding the highly variable EMP1 genes, 10 genes have nonsynonymous SNPs (Table S8). Within these ten genes, *samc*, *ftsh1*, *thzk* were selected as top candidates (Fig. 3a) as they possess nonsynonymous SNPs that have been observed in the field, are expressed in the asexual blood stages[66], and have been previously associated with antiplasmodial resistance to the preclinical candidates MMV019662, MMV028038[67] and actinonin[68,69]. *samc* is predicted to be essential in *P. falciparum* and *P. berghei* and have a fitness cost in *P. falciparum*, *ftsh1* is predicted to be dispensable in *P. falciparum* with no fitness cost, and *thzk* is predicted to be dispensable in *P. falciparum* and may have a slight fitness cost (this gene does not have an ortholog in *P. berghei*).

We also examined the field prevalence of the Cam3.II SNP positions in these genes using the clinical isolate genomes from the Pf3k database (Extended Data 6b-d). FtsH1 D695G was observed in Southeast Asian countries and not in Africa. The SAMC I176K/R (K observed in Cam3.II) / S193A/P/T (A observed in Cam3.II) haplotype was observed at a high prevalence, especially in Southeast Asian countries compared to African countries. The single I176K/R or S193T/P/A was observed at low prevalence, and the WT I176 / S193 haplotype was not observed. The most probable reason the chromosome 12 QTLs were not detected in previous studies is that the Cam3.II (QN-resistant) alleles for our top candidate genes *ftsh1*and *thzk* were not present in the previous HB3 (Honduras), Dd2 (Indochina), 7G8 (Brazil), and GB4 (Ghana) cross parents (sequence data for *samc* were not available for these parasites on PlasmoDB).

FtsH1 is a potential mediator of QN resistance and modulator of CQ and md-CQ resistance

To investigate whether the chr 12 QTL candidates, *samc* and *ftsh1* play a role in md-CQ, CQ, and QN response, we genetically-edited the Cam3.II parasites to revert the mutant alleles to WT in these genes (Supplemental Fig. 3, with slight modifications). Due to the

low complexity of the *samc* gene, the donor was not cloned into the 'all-in-one' CRISPR/Cas9 plasmid and was instead co-transfected in a separate plasmid. All primers used for cloning and verification in this paper are described in Table S11 and all generated plasmids are described in Table S12.

For the *samc* and *ftsh1*-edited lines, we tested for significant shifts in susceptibility to QN, md-CQ, and CQ by comparing the IC_{50} and IC_{90} values of the reverted lines (denoted as *samc*^{WT} or *ftsh1*^{WT}) to the unedited parent (Fig. 4a-f). We found that reverting *ftsh1* to WT in Cam3.II caused significant sensitization at the QN, md-CQ, and CQ levels. These results suggest that *ftsh1* can act as a potential contributor to QN resistance and a possible modulator of CQ and md-CQ resistance. Nonetheless, the lack of a strongly significant shift at the CQ IC_{50} level is consistent with *ftsh1* not being a primary driver of resistance to CQ. PfFtsH1 is a membrane metalloprotease that is homologous to the bacterial membrane AAA+ metalloprotease[70]. PfFtsH1 was shown to be required for apicoplast biogenesis, which was postulated to involve proteolysis regulation of critical apicoplast membrane protein(s)[68]. In the D10 *P. falciparum* parasite genetic background, FtsH1 G489C (located in the peptidase domain) conferred resistance to actinonin. The D695G SNP in Cam3.II is predicted to be outside the domain and there was no statistically significant difference between the FtsH1 WT NF54 and D695G Cam3.II actinonin IC_{50} values (data not shown), suggesting that D695G may not be involved directly in the FtsH1 protease activity.

When we compared the *samc*^{WT} md-CQ IC_{50}, IC_{90}, and CQ IC_{90} values with the unedited Cam3.II parent, there was no statistically significant shift, indicating that *samc* is most likely not a mediator driving the chr 12 QTL peak. We also profiled the *samc*^{WT} against LMF but did not see a statistically significant shift compared to the unedited Cam3.II parent (data not shown). Given that the 146kb md-CQ chr 12 IC_{90} and CQ QTLs matched the QN IC_{90} QTL and was encompassed in the QN IC_{50} QTL, we initially hypothesized that they were most likely driven by the same gene. We cannot ignore, however, the possibility that the 136kb larger QN IC_{50} chr 12 peak may in fact involve an additional mediator compared to md-CQ and CQ.

dmt1 is a top candidate for mediating QN resistance

Of the 82 genes within the QN IC_{90} QTL region, 33 genes harbored nonsynonymous SNPs that distinguished the parents, with the QN-resistant Cam3.II having the mutant alleles. DMT1 is of particular interest as it is annotated as a putative drug/metabolite transporter, and is predicted to be structurally similar to PfCRT. They are both members of the drug/metabolite exporter (DME) family within the DMT superfamily. DMT1 is predicted to be a 434-amino acid-long membrane transporter with 9 or 10 transmembrane domains based on TMHMM[71] and TMpred analyses[72], respectively (data not shown), while PfCRT is 424 amino acids in length and has ten transmembrane domains. The Y107 and S129 positions are predicted to not reside in the transmembrane helices. We calculated the structural similarity between the AlphaFold-predicted NF54 DMT1[73] and cryo-EM derived 7G8 PfCRT[74] via ChimeraX MatchMaker (Extended Data 7). This comparison revealed a good alignment of 1.271Å between 47/300 pruned atom pairs (predicted to be in the transmembrane domains). However, the overall alignment across

all 300 atom pairs was poor (20.175Å) most likely due to the flexible regions that are annotated by AlphaFold as “very low confidence” regions, where the Y107N and S129L mutations reside.

Y107N and S129L mutations were not observed in the previous genetic cross parents that were used to investigate QN resistance, possibly providing a reason for why DMT1 has not been associated with resistance to QN. Broadening the examination of *P. falciparum* strains, we examined the SNPs at the Y107 and S129 positions from the set of 2,512 strains in the Pf3k database, covering six Asian and eight African countries (Extended Data 6a). While Y107N mutations were observed in all countries, S129L was only observed in Cambodia, Laos, Myanmar, Thailand, and Vietnam, only if they already possessed the Y107N mutation. This suggests that the S129L may have arisen later, on the already Y107N mutant genetic background. Of note, the Pf3k database does not contain South American parasite genomes, which would have been insightful as QN was first discovered and QN resistance was first reported in this region. Furthermore, QN is still used today as part of the 2022 antimalarial drug policy for severe malaria in French Guiana and Guyana (with artesunate or clindamycin) as well as IPTp in French Guiana[1].

We also conducted a protein-level multiple sequence alignment between *P. falciparum* NF54 DMT1 and its orthologues in representative reference strains of twelve other *Plasmodium spp.* for rodent, avian, laverania (human ape-infecting), human, and primate / human malaria using the PlasmoDB database[75] and Clustal Omega (Supplemental Fig. 2a). Strong conservation was observed in the TMHMM-predicted DMT1 transmembrane domains. Phylogenetic trees (Supplemental Fig. 2b) revealed that *P. falciparum* DMT1 was the most similar to DMT1 orthologues in *P. reichenowi*, *P. adleri*, and *P. gaboni*, which are also laverania malaria species and appear to share evolutionary ancestry, which is consistent with *P. falciparum* originating from gorillas[76]. Interestingly, *P. reichenowi*, *P. adleri*, *P. gaboni*, and *P. falciparum* show a fully conserved region from I100–S106, and while NF54 *P. falciparum* has Y107, the other strains possess the Y107N observed in Cam3.II (all four strains share S129). While the *dmt1* gene has been minimally examined in literature, *dmt1* was predicted to be potentially dispensable as it was mutable in the CDS and to have a fitness cost (Fig. 3a) in a *piggyBac* transposon insertion mutagenesis screen[77]. In *P. berghei*, *dmt1* (*Pb*ANKA_1422100) was predicted to be dispensable (*Plasmo*GEM) KO screen[78] and validated in a genetically-edited DMT1 KO parasite[79] but it may have a potential defect in mosquito-to-mouse transmission[80].

Mutant DMT1 appears to play a modulatory role in parasite susceptibility to QN

To investigate whether DMT1 is a modulator of QN susceptibility *in vitro*, we edited the DMT1 locus at the Y107 and S129 positions (mutate to Y107N / S129L or revert to wild type) in the parents and select progeny (Supplemental Fig. 3). We selected the NF54 and Cam3.II parents, as well as the B-QN95-140-A5 (H079), B4-5 (H030), C-QN95-180-F8 (H071), B-CQ75-1-H9 (H062), and B5-4 (H046) progeny for SNP editing, based on their genotypes in *dmt1*, *pfcrt*, *thzk*, *ftsh1*, *samc*, and the chr 2 QTL locus (Table S7) and their susceptibility to QN (Fig. 1c,d). Of note, of the progeny profiled, H071 exhibited the highest QN IC_{50} value. We conducted drug assays on the DMT1 SNP-edited lines and their unedited parental parasites (Fig. 5a). A statistically significant sensitization to QN

was observed between the SNP-edited lines and their unedited parasites only for H079. There was, however, a trend of the Cam3.II and H071 DMT1 revertants (*dmt1*^{WT}) having a lower QN IC_{50} than the unedited strain (~20% and 19%, respectively). One possible explanation for the lack of statistical significance is that we have observed that the QN-resistant parasites are more susceptible to variability in their QN response, compared to less sensitive lines, and that we may need more biological replicates to achieve a statistically significant difference between the revertants and the unedited controls. Given the lack of a significant shift in the DMT1 Y107N / S129L-mutated NF54 and the lack of a full sensitization in Cam3.II DMT1 revertants, DMT1 alone does not cause resistance or sensitization to QN, as expected of QN resistance being a multigenic trait. In the H062 and H046 progeny (both Dd2 PfCRT, DMT1 WT), mutating DMT1 to Y107N / S129L did not cause a shift in QN susceptibility, suggesting that genetic background plays a role in QN response and that there are other non-*pfcrt* and non-*dmt1* genes involved. As we saw with Cam3.II, however, the DMT1 Y107N / S129L allele did appear to play a modulatory role in parasite susceptibility to QN.

We also profiled the same DMT1 SNP-edited lines and their unedited parasite controls against md-CQ and CQ, and the Cam3.II-edited parasites against md-ADQ (negative control) (Supplemental Fig. 4). We did not observe any statistically significant differences between the SNP-edited lines and their unedited controls in their response to md-CQ, CQ, and md-ADQ for all but H071. H071 DMT1 revertants became less susceptible to CQ and md-CQ than their unedited controls, possibly due to an altered interaction with another gene in this genetic background. Specifically, in the Cam3.II parasites, we did not observe any pattern of the revertants becoming more sensitive than their unedited controls against md-CQ, CQ, and md-ADQ, unlike our findings for QN, suggesting that the modulatory role of DMT1 is mostly QN-specific.

Phenotypic profiling of DMT1 knockout strains validates DMT1 as a marker of QN resistance

To further investigate the role of DMT1 in QN resistance and examine if DMT1 expression levels cause shifts in QN susceptibility, we generated DMT1 KO parasites in the QN-resistant Cam3.II genetic background (Supplemental Fig. 5). We profiled four different Cam3.II DMT1 KO parasites, as well as the unedited Cam3.II and the QN-sensitive NF54 parents, against QN (Fig. 5b,c). We found that the DMT1 KO significantly sensitized Cam3.II to QN at the IC_{50} and IC_{90} levels, validating DMT1 as a mediator of QN resistance. The sensitization was by ~25% and ~30%, respectively, indicating that other mediators are required for the QN resistance phenotype. We also profiled the KO parasites against MFQ, LMF, CQ, md-CQ, and md-ADQ to test for cross-resistance—i.e., whether DMT1 mediates resistance to other antimalarials—and to confirm that the shift in susceptibility was drug specific. Intriguingly, we found that deleting DMT1 did not sensitize Cam3.II to any other drug beside QN at the IC_{50} level (Fig. 5b). The DMT1 KO did, however, significantly sensitize Cam3.II to MFQ, LMF, and CQ at the IC_{90} level, although the shifts were much smaller compared to those seen for QN. These results are not surprising, as QN, MFQ, and LMF are all classified as aryl-amino alcohols (Extended Data 1a) and have been suggested to share resistance mechanisms[21-24].

DMT1 localizes to the digestive vacuole, lipid bodies, parasitophorous vacuolar membrane, as well as structures associated with vesicular trafficking

To shed light on potential functional role of DMT1 in the parasite, we investigated the subcellular localization of DMT1, as its location has not been elucidated to date in any *Plasmodium spp.* We generated DMT1-3×HA-tagged parasites in the NF54 genetic background (Supplemental Fig. 6a), which we confirmed by PCR and Sanger Sequencing, as well as by western blot using parasite lysates probed with an anti-HA antibody (Supplemental Fig. 6b). We conducted widefield deconvolution confocal microscopy of our DMT1-3×HA-tagged parasites by indirect IFAs and probed for DMT1 using anti-HA antibodies. We observed DMT1 expression in all asexual blood stages, but used the trophozoite-stage parasites for quantifying colocalization of DMT1 with organelles as there were more spatial distribution of organelles than in rings and were less prone to variability than the multinucleated schizonts. DMT1 consistently exhibited a punctate shape at all parasite stages, possibly indicative of involvement in vesicular trafficking.

To further investigate the DMT1 subcellular localization, HA-counter-stained parasites were co-stained with markers for the mitochondria (MitoTracker Red CMXRos), apicoplast (PfACP), late endosome (Rab7), early endosome (Rab5B), post-Golgi (Rab11A), ER (BiP), PVM (PfEXP2), DV (PfCRT and PfPM2), and lipid bodies (Nile Red). Parasites were also co-labeled with antibodies for PfK13, the ART resistance mediator that was previously localized to the neck of cytostomes at the plasma membrane, the ER, and internal vesicular structures[81-83]. Representative images and their three-dimensional renderings are shown in Fig. 6a-g, Extended Data 8. If DMT1 colocalization with the marker was binary (sometimes colocalizing and other times not), then we chose an image representing both localization patterns. Colocalization was quantified as the mean percentage±SEM of DMT1-3×HA volume above threshold colocalized as well as the mean±SEM Manders' coefficient for DMT1-3×HA (Table S15, Extended Data 8j). As DMT1 consistently did not colocalize with the mitochondria (1.5±0.6%) (Extended Data 8a), Student's *t*-tests that compared localization of DMT1 with organelles vs DMT1 with the mitochondria were used to calculate *p* values. DMT1 also did not colocalize with the apicoplast (10.5±5.4%) (Extended Data 8b). This was an unexpected result as *P. falciparum* DMT2 (another DMT superfamily protein) colocalized with the apicoplast[79].

Another striking finding was the significant colocalization of DMT1 with DV membrane markers (29.2±8.0%, 16.7±2.5%) (Fig. 6f, Extended Data 8f,g). While the percent localization and thresholded Manders' coefficient are not as high for some other organelles, most likely because DMT1 only partially overlapped with the DV membrane, we did see a pattern of DMT1 overlapping with the DV membrane. DMT1 either almost fully (>80%) colocalized with lipid bodies (Nile Red) (43.6±10.8%) (Fig. 6g, Extended Data 8h), the ER (39.8±10.3%) (Fig. 6c, Extended Data 8d), and the PVM (40.9±12.4%) (Fig. 6e, Extended Data 8e), or minimally colocalized. This discrepancy may be due to DMT1 being trafficked within the parasite. Interestingly, Nile Red has been shown to localize to DV-adjacent small cytoplasmic neutral lipid droplets that contain di- and triacylglycerols in *P. falciparum*, which may explain why we observed colocalization with both Nile Red and PfCRT[84-86]. In addition to the DMT1 colocalization with the ER, DMT1 also partially

colocalized with the early endosome (27.9±7.2%) (Fig. 6b, Extended Data 8c), and less so with the late endosome (10.2±5.7%) (Fig. 6a) and post-Golgi (10.8±4.5%) (Extended Data 8i), potentially implicating DMT1 in the vesicular trafficking pathway. In further support of this thought, DMT1 significantly colocalized with K13 as well, which colocalized with the cytostomes, the ER, and vesicular structures[81-83]. We posit that DMT1 may be trafficked by vesicular structures from the direction of the PVM to the DV, with its final localization/site of action potentially being on the DV membrane or at the DV-adjacent lipid bodies. At the latter site, DMT1 may be involved in lipid storage of phospholipids digested in the DV and/or indirectly involved in the heme detoxification pathway, as di- and triacylglycerols have been shown to promote β-hematin formation.

NF54 and Cam3.II DMT1 isoforms differentially transport [^{3}H]QN

Given that DMT1 is annotated as a putative drug/metabolite transporter and is structurally similar to PfCRT, shown to partially inhibit heme detoxification, localize to the DV, lipid bodies, PVM, and vesicular trafficking structures, we were interested in determining whether DMT1 can transport QN, similar to how DV-localized PfCRT transports CQ. We purified and reconstituted NF54 (WT) and Cam3.II (Y107N / S129L) DMT1 isoform proteins in proteoliposomes and measured their uptake of [^{3}H]QN and [^{3}H]CQ (Fig. 6h,i). Notably, we observed that both DMT1 isoforms can transport both [^{3}H]QN and [^{3}H]CQ, however, a statistically significant difference in uptake was observed only with regards to [^{3}H]QN. These data provide a possible mechanistic explanation that links DMT1 as a potential transporter of QN, and that QN mechanism of action and resistance may, in part, be mediated by altered DMT1-mediated QN transport. In addition, NF54 (WT) and Cam3.II (Dd2) PfCRT isoforms were also shown to transport [^{3}H]QN and [^{3}H]CQ, although the complete loss of uptake signal in NF54 PfCRT was only seen for the latter drug. These results are in line with previous studies partially associating *pfcrt* with QN resistance, and observations of PfCRT transporting non-CQ drugs, thereby impacting the parasite response to these drugs by potentially changing the drug concentration at their site of action[27].

Discussion

In summary, we have conducted a NF54 × Cam3.II *P. falciparum* genetic cross to map determinants of resistance to CQ and QN, by applying phenotypic and genomic analyses to most of the 120 independently obtained, unique recombinant progeny. We show that applying different selective pressures (including different concentrations of the same drug) to bulk progeny pools, prior to progeny cloning, helped us to enrich for 65 new unique recombinants, compared to the set of 55 recombinants that we obtained without drug pressure.

Pressuring progeny bulk progeny pools with CQ and QN which both harbor a 4-aminoquinline ring, yielded several interesting insights into their mechanisms of resistance. As only 5 out of the 120 unique recombinant haplotypes were obtained in both CQ and QN selections, we were able to postulate that there is minimal overlap in their resistance mechanisms, and that distinct mediators are most likely involved. Delving into the gene-level, we also examined the parental allele frequencies in *pfcrt*, which is known to be the primary driver of resistance to CQ, and which has earlier been partially

associated with QN resistance. We were able to confirm our finding of distinct resistance mechanisms between CQ and QN, as mutant *pfcrt* was observed in 100% of CQ-selected haplotypes, compared to only 21% in QN-selected haplotypes. We also applied both a bulk selection approach and a progeny clone-based approach to further investigate QN resistance. In both analyses, we were able to find statistically significant QN QTL on chromosome 7, however, the bulk segregant analysis was prone to more variability. This caveat made it especially challenging to use bulk segregant analysis as a sole method to study multigenic traits such as QN resistance, where detection of multiple QTL peaks is critical, and thus progeny-based QTL analyses were pursued.

In our CQ and md-CQ progeny clone-based QTL analysis, we identified a novel chromosome 12 QTL that overlapped with the QN chromosome 12 QTL. We identified *ftsh1, thzk, and samc* as the top candidates from our QN, CQ, and md-CQ chromosome 12 QTLs, given the presence of SNPs in the Cam3.II resistant parent, expression in the asexual blood stage, SNPs being observed in the field, and the genes previously being associated with resistance. Our SNP-editing data revealed *ftsh1* as a potential mediator of QN resistance and a potential modulator of CQ and md-CQ resistance, as the Cam3.II *ftsh1 D695G*^{WT} parasites became significantly less sensitive to these drugs compared to the unedited Cam3.II strain.

We identified DMT1 as the top candidate from our QN IC_{90} chromosome 7 QTL, which was only ~4kb upstream of the QTL peak (and 230kb downstream of *pfcrt*). In support of its prioritization, the QN-resistant Cam3.II parent harbors SNPs (Y107N / S129L), the gene is expressed in asexual blood stage parasites, and the protein is structurally similar to the related drug/metabolite exporter family protein, PfCRT. DMT1 may not have been detected in prior genetic cross studies as none of those parents harbored the Y107N / S129L SNPs and because multigenic resistance traits may require phenotyping of a large number of progeny such as the >90 examined in our study, whereas previous studies have generally studied 30 to 40 progeny[18,19]. We validated DMT1 as a component of a multigenic trait of QN resistance, as our data revealed that deleting this gene significantly sensitized Cam3.II (by ~25%) at the IC_{50} level against QN, but not against MFQ, LMF, CQ, md-CQ, or md-ADQ. Our DMT1 SNP-editing studies demonstrated that the QN resistance mechanism, as well as the contribution of DMT1, remains complex. We observed a trend of Cam3.II DMT1^{WT} parasites exhibiting a ~17% shift in susceptibility compared to their unedited parent, and 20-40% shift in two progeny genetic backgrounds and none in another. We may have seen a larger shift in QN response in our Cam3.II DMT1 KO parasites compared to the Cam3.II DMT1 SNP-edited parasites because the level of DMT1 protein expression may also be important for mediating QN resistance. An analogous situation was earlier observed with PfCRT where reducing the protein expression level (by introducing a truncated 3' UTR) led to a similar reduction in CQ IC_{50} in CQ-resistant parasites[87]. We could not test this hypothesis herein as we lack an anti-DMT1 antibody that can probe differences in DMT1 protein levels. We also observed no significant shift when mutating DMT1 to Y107N / S129L in NF54 (expressing WT *pfcrt*), B5-4 (*pfcrt* Dd2), or B-CQ75-1-H9 (*pfcrt* Dd2), suggesting that genes besides *dmt1* and *pfcrt* are also necessary for conferring QN resistance. Our finding that *pfcrt* alone did not drive QN resistance was consistent with another prior study in which a conditional

knockdown of PfCRT significantly sensitized a CQ- and QN-resistant Dd2 parasite to CQ and md-ADQ (as measured by IC_{50} and drug uptake) but not to QN[88]. Of note, *pfcrt* was only 62kb upstream of the QN IC_{50} QTL peak center and was included in the QN IC_{90} peak, suggesting that *pfcrt* is a contributor to QN response in this genetic background and that further investigation to elucidate its contribution to QN response in relation with *dmt1* is warranted.

To postulate how DMT1 may be mediating QN resistance, we examined both DMT1 and QN. As QN has been previously partially implicated in the heme detoxification pathway[54], we directly tested this potential mode of action *in vitro* using a β-hematin inhibition assay. We found that QN inhibits hemozoin formation to a lesser degree than CQ, but more so than MFQ. We also compared structural similarities of QN and other antimalarial compounds and observed that QN was the most similar to MFQ. Previous reports have indicated that MFQ and QN act through overlapping mechanisms[24] that include the inhibition of heme detoxification (β-hematin crystal growth measured by *in situ* atomic force microscopy)[54]. These drugs have also been suggested to target the *P. falciparum* purine nucleoside phosphorylase (PfPNP) based on cellular thermal shift assays[21]. Other studies, however, have reported mechanisms that are unique to each drug[89-91]. In addition, overlapping and discrepant resistant mechanisms between QN and MFQ have been revealed by the profiling of genetically-edited or *in vitro* drug-selected parasites for *pfmdr1*[22,23] and *pfcrt*[34]. Our studies and those by others suggest that the role of DMT1 in QN and possibly MFQ resistance should be investigated further through gene editing studies in other genetic backgrounds.

We also revealed the subcellular localization of DMT1 in a *Plasmodium* species for the first time. DMT1 localized to the DV, lipid bodies, the PVM, and structures associated with vesicular trafficking as evidenced by partial Rab5B and ER staining. Our results suggest that DMT1 may be trafficked by vesicular structures from the direction of PVM to the DV, either to the membrane or in DV-adjacent lipid bodies. As speculated upon above, DMT1 might be involved in storing phospholipids in the DV and/or be indirectly involved in the heme detoxification pathway, as di- and triacylglycerols have been shown to promote β-hematin formation[86,92]. Furthermore, we were able to link QN and DMT1 functionally, by showing that NF54 and Cam3.II DMT1 isoforms can transport [^{3}H]QN in DMT1-loaded proteoliposomes. Furthermore, the Cam3.II DMT1 isoform showed statistically significant higher levels of [^{3}H]QN uptake, compared to the WT NF54 isoform, suggesting that mutant DMT1 can contribute to QN resistance via intracellular flux away from its site of action. We note that the directionality is uncertain, as QN can to a degree affect heme detoxification that occurs primarily in the DV but is also suspected to have additional targets that may be outside the DV[93].

Future studies should include editing multiple QN resistance mediators in the same parasite line to examine whether in combination they are able to fully sensitize parasites or render them QN-resistant. In addition to the chromosome 7 and 12 peaks, a smaller QTL on 6 was observed and the gene(s) driving these QTLs will require further investigation. Another future avenue is to genetically edit candidate genes in strains other than NF54 and Cam3.II, using either SNP or KO/cKD approaches. This work should focus

on parasites from regions where QN is used, as well as parasites exhibiting high-grade resistance to QN (Cam3.II showed a moderate level of resistance), to examine the role of parasite genetic backgrounds in QN response.

First-line treatments are updated whenever their therapeutic efficacy decreases below 90%. As QN usage is likely to increase as partial resistance to ART spreads, there is an urgent need to identify markers of QN resistance to detect and monitor its emergence or spread. Our data suggest that *dmt1* should be sequenced in clinical isolates, especially in regions where QN is still widely used (e.g. Mali)[94] and in samples from cases of QN treatment failure. Our analysis of the Pf3k database showed that the S129L SNP was only observed in countries in Southeast Asia and not Africa (in samples collected until around 2012). It would be very interesting to know whether S129L is now present in African countries, as QN is still being used in some regions as an alternative to artesunate[4]. Also, the recent emergence of ART-resistant mutant K13 parasites in east Africa (including Uganda, Rwanda, Eritrea, Ethiopia, Tanzania[3], and Sudan (unpublished)) raises the prospect of increased QN in these areas to treat severe malaria in the pediatric population. Thus, the QN resistance markers identified in our study are likely to be of increasing importance in the coming years.

Lastly, our QN studies highlight the value of using antimalarial compounds with complex modes of actions and resistance for treatment. Despite QN being the oldest antimalarial drug, it remains effective to this day, most likely because the parasite must develop mutations in multiple genes to acquire resistance. In future drug discovery efforts, chemical compounds that have multiple *P. falciparum*-specific targets and/or multiple resistance mediators merit prioritization for clinical use.

Methods

Parasite *in vitro* culture. Asexual blood stage *P. falciparum* parasites were cultured in human RBCs obtained from the Interstate Blood Bank (Memphis, TN) or New York Blood Center (New York, NY) at 3% hematocrit, using RPMI 1640 supplemented with 25mM HEPES, 2.1g/L sodium bicarbonate, 10mg/mL gentamicin, 50mM hypoxanthine, and 0.5% (w/v) AlbuMAX II (Thermo Fisher Scientific). Parasites were maintained at 37°C under 5% O_2/ 5% CO_2/90% N_2 gas conditions.

Genomic DNA (gDNA) extraction. Parasite genomic DNA was obtained from cultures at 5 to 10% parasitemia with mostly trophozoite and schizont stages. Red blood cells were lysed with 0.1% saponin in 1×PBS and parasite DNA extracted with the QIAamp DNA Blood Midi Kit (Qiagen) using a combined RNase and Proteinase K treatment. DNA concentrations were determined using NanoDrop and/or the Qubit dsDNA BR assay kit (Thermo Fisher Scientific).

Parasite drug-susceptibility assays. Parasites were synchronized for at least two consecutive ABS cycles prior to starting drug susceptibility assays and at least once a week thereafter, by exposing asexual blood stage cultures to 5% D-Sorbitol (Sigma) for 15–20min at 37°C to remove mature parasites, followed by a wash step. In drug susceptibility assays, predominantly ring-stage parasites were exposed to a serially

diluted range of drug concentrations (twofold, ten-point for all drugs but QN, and twelve-point for QN), or 700nM DHA (kill control) or no drug control, starting at 0.2% parasitemia and 1% hematocrit in 96-well flat-bottom plates. The assay plates were incubated at 37 °C for 72h in 5% O_2/5% CO_2/90% N_2. Final parasitemias were measured using a BD Accuri C6 Plus cytometer with a HyperCyt plate sampling attachment (IntelliCyt), an IntelliCyt iQue Screener Plus cytometer (Sartorius), or a BD FACSCelesta flow cytometer with the BD High Throughput Sampler (HTS). Cells were stained with 1×SYBR Green I (Invitrogen) and 100nM MitoTracker DeepRed FM (Invitrogen) for at least 20min and diluted in 1×PBS prior to sampling. Parasitemia in each well was determined as the percentage of MitoTracker positive SYBR Green I positive infected red blood cells within the cell subpopulation gated in the FSC vs SSC plot. Parasitemia was then normalized by subtracting the background parasitemia in the 700nM DHA kill control, and 50% inhibitory concentration (IC_{50}) and 90% inhibitory concentration (IC_{90}) values were calculated by nonlinear regression analysis (Prism version 10, GraphPad). Drug-susceptibility assays were performed with QN, CQ, monodesethyl-Chloroquine (md-CQ), monodesethyl-Amodiaquine (md-ADQ), LMF, and MFQ. Statistical significance was determined by nonparametric, two-tailed Mann–Whitney *U*-tests for QN, CQ, and md-CQ QTLs and Student's t-tests for all other drug assays using Prism version 10 (GraphPad) software.

Genetic cross. NF54 and Cam3.II *P. falciparum* gametocytes were cultured as previously described[95]. Briefly, parasites were propagated in RPMI 1640 media containing 10% v/v human serum, at 4% hematocrit and 37°C in a glass candle jar. Cultures were initiated at 0.5% asynchronous asexual parasitemia from a low-passage stock and maintained up to day 18 with daily media changes but without any addition of fresh RBCs. Day 15 to 18 cultures, containing largely mature gametocytes, were used for mosquito feeds. Cultures were centrifuged (108×g, 4 min) and the parasite pellet was adjusted to 0.6% gametocytemia in a mixture of human O+ RBCs supplemented with 50% v/v human serum. To conduct a genetic cross between NF54 and Cam3.II, we used a 1:1 ratio of gametocytes at a final gametocytemia of 0.6%. Gametocytes were fed for one hour to 4- to 6-day old *Anopheles stephensi* mosquitoes (Liston strain) that had been starved overnight, using glass membrane feeders. Unfed mosquitoes were removed after feeding. Fed mosquitoes were then maintained on a 10% sugar solution at 25°C and 80% humidity with a 14:10h (light:dark) cycle including a 2h dawn/dusk transition. Human RBCs used to set up the cultures were collected weekly from healthy volunteers, with informed consent, under a Johns Hopkins University Institutional Review Board approved protocol (number NA_00019050). All experiments were performed in accordance with institutional guidelines and regulations.

On day 7 post-infected blood meal, mosquito midguts were harvested and stained with mercurochrome. Oocysts were counted by brightfield microscopy using a Nikon E600 microscope with a PlanApo 10× objective. We observed a ~85% prevalence of infection, with an average of ~20 oocysts per mosquito. Between days 14 to 16, salivary glands were harvested from ~35 mosquitoes, homogenized and the sporozoites counted using a hemocytometer. On average we obtained 40,000 salivary gland sporozoites per mosquito.

All animal experiments were performed in accordance with the Animal Care and Use Committee (ACUC) guidelines and approved by the Johns Hopkins ACUC (Protocol M017H325), with modifications to a protocol reported previously[47]. FRG NOD human liver-chimeric (huHep) mice[48] were purchased and shipped from Yecuris Corporation. Upon arrival we began withdrawal of the mice from 2-(2-nitro-4-trifluoromethylbenzoyl)-1,3-cyclohexanedione (NTBC). Mice were housed in a sterile facility with sterile bedding, food, and water. Mice were weighed daily and those that showed any weight loss >10% (compared to pre-shipment weight) were treated with 300 μL of sterile saline via intraperitoneal injection and given a nutritional supplement in water (STAT; https://www.prnpharmacal.com/products/nutritional-supplements/stat/). Prior to infection, mice were allowed to recover from shipping for 2 to 3 days. Infection with *P. falciparum* sporozoites was performed either by mosquito bite or by intravenous (IV) inoculation. For the mosquito bite approach, mosquitoes were allowed to probe/feed for 17 to 19 min on mice anaesthetized with 150μL ketamine/xylazine. Two mice (A and B) each received mosquito bites from approximately 60 mosquitoes. Two other mice (C and D) were given prophylactic penicillin/streptomycin antibiotics and then IV-inoculated with 200,000 sporozoites dissected from mosquito salivary glands. Mice infected by IV inoculation remained stable and healthy appearing for the remainder of the experiment. In contrast, both mice infected by mosquito bite lost 5–6.5% of their body weight relative to their pre-shipment weight and were given extra rehydration gel food. On days 5 and 6 post-sporozoite infection, 450–500μL of RPMI-washed human RBCs at ~70% hematocrit were IV-inoculated into each mouse (except for IP-injection for Mouse B due to scar tissue at the tail vein injection site). Mice were given new dextrose, cages, and rehydration gel food on both days. At day 7 post-infection, ABS parasites were detected at 0.33–0.76% parasitemia and blood was recovered by cardiac puncture of mice anesthetized with ketamine/xylazine (Table S1). Bulk freezes were made after one and two cycles in culture. The bulk freezes post-one cycle were thawed from each mouse and used to obtain progeny clones by limiting dilution cloning (referred to as clones from no drug pressure prior to cloning). The post-two cycle freezes for mice B and C were later thawed and pressured at CQ 50nM, CQ 75nM, QN 75nM, or QN 95nM for 3 days in 5mL cultures at 3% hematocrit. Surviving parasites were then cloned and cryopreserved. Mouse B 'no drug', as well as mouse B and C QN 95nM pre-selected bulks, were thawed and pressured at QN 0nM, 140nM (and later 240nM), or 180nM (and later 240nM) for 4 days for bulk selection experiments, and the drug-pressured bulks were cloned by limiting dilution and cryopreserved.

Parasite strains and progeny cloning. The Cam3.II G8 parasite is a clone of the Cam3.II parasite (also known as RF967 and PH0306-C) kindly provided by Dr. Rick Fairhurst (then at the NIH). NF54 JHU, Cam3.II G8 genetic cross parental and progeny strains were cultured in human RBCs were obtained from the Interstate Blood Bank (Memphis, TN) or the New York Blood Center (New York, NY). Parasite cultures were maintained at 3% hematocrit, using RPMI 1640 media supplemented with 25mM HEPES, 2.1g/L sodium bicarbonate, 10mg/mL gentamicin, 50mM hypoxanthine, 0.5% (w/v) AlbuMAX II (Thermo Fisher Scientific), and 10% (v/v) human serum (Interstate Blood Bank). Parasites were maintained at 37°C under 5% O_2/5% CO_2/90% N_2 gas conditions.

After cloning by limiting dilution, parasites were adapted to the aforementioned media now devoid of 10% human serum, and all phenotyping was conducted in this serum-free media.

Whole-genome sequencing (WGS) of genetic cross progeny pools and clones. Parasite samples were subjected to WGS using the Illumina Nextera DNA Flex library preparation protocol. Briefly, 150ng of gDNA was fragmented and tagmented using bead-linked transposons and subsequently amplified by five cycles of PCR to add dual-index adapter sequences to the DNA fragments. The libraries were quantified, pooled, and sequenced on Illumina MiSeq (paired-end 300bp reads) or NextSeq (paired-end 150bp reads) platforms.

Progeny were sequenced either directly (for bulk pools and clones after QN 140nM, 180nM, and 240nM pressure) or after clonal recombinants had been identified by microsatellite and SNP genotyping (for clones following no drug pressure or CQ 50nM, CQ 75nM, QN 75nM, and QN 95nM pressure). The WGS data for the parents and progeny clones are visualized in Fig. 1b. Sequence data were aligned to the *P. falciparum* 3D7 genome (PlasmoDB version 48) using Burrow-Wheeler Alignment (BWA)[96]. Reads that did not map to the reference genome and PCR duplicates were removed using SAMtools and Picard. The reads were realigned around indels using Genome Analyses Tool Kit (GATK) RealignerTargetCreator and base quality scores were recalibrated using GATK BaseRecalibrator.

Using SAMtools mpileup, variants were called and filtered based on quality scores (minimum base quality score ≥20, mapping quality >30, read depth ≥5) and multiallelic = FALSE to obtain high-quality SNPs that were annotated with SnpEff[97]. SNPs for highly polymorphic surface antigens and multi-gene families were removed. Homozygous SNPs that differed between the NF54 and Cam3.II parents were retained, defined as having >90% alternate or reference allele frequency for NF54 or Cam3.II, respectively. We further culled these loci if more than 16 out of 214 progeny (approximately 7%) contained SNPs classified as heterozygous (allele frequency of >10% and <90%) or missing (no reads or reads that did not pass the variant caller's quality filter, or DP<5), to retain 12,547 high quality SNP loci.

Microsatellite sizes in the NF54 and Cam3.II parental strains were identified as described previously[98]. Briefly, to determine the confidence of a microsatellite based on the number of reads, a custom Python script utilizing the pysam[99] module was written to call reads that harbored insertions or deletions at specified genomic loci within the respective windows. Integrative Genomics Viewer was used to verify the data.

Identification of unique recombinants. PCR and gel electrophoresis microsatellite genotyping (n=11 markers; Table S3) was used to narrow down which of the 175 progeny obtained after no drug pressure were clonal recombinant progeny, before their gDNA was whole-genome sequenced. 296 out of 303 progeny obtained after CQ 50nM, 75nM and QN 75nM and 95nM selections were genotyped with nine markers: two sets of three microsatellite markers via multiplexed capillary electrophoresis-based genotyping (Table

S3), and three SNPs in *pfcrt* (A220S), *dhfr* (N51) and *pfmdr1* (Y184F) were used to screen for clonal recombinant progeny before their gDNA was whole-genome sequenced. Seven progeny had their gDNA directly genotyped by WGS. To increase the chance of obtaining highly QN-resistant progeny, cloning plates set up after QN 140nM, 180nM and 140+240nM selections were split 1:2 with one plate pressured with no drug and the other pressured with QN 140nM for three days to predict which of the 160 progeny were most likely not resistant (defined as <1× expansion in drug and/or <30% live parasites in drug/no drug control). The gDNA for the remaining progeny was sent for WGS.

To identify which progeny were isogenic and to assign haplotypes to the progeny, WGSs of the parents and clonal progeny at the 13,116 high quality SNP positions were hierarchically clustered by average linkage using Gene Cluster 3.0[100]. The resulting dendrograms were visualized using Java TreeView[101]. The SNP inputs were as follows: NF54 allele = -3, Cam3.II allele = 3, heterozygous or missing = 0. Clustering of the unique recombinant haplotypes and parental haplotypes were also conducted. If there were isogenic progeny with the same haplotype, then the sequence for the progeny with the best sequencing data (lowest percentage of mixed and missing SNP calls) was used as the representative haplotype for subsequent clustering analysis.

Quinine bulk segregant analysis. Recombinant bulk pools from Mouse B and C (with or without prior QN 95nM drug pressure) for the NF54 JHU×Cam3.II G8 cross were used for QN BSA experiments (full sample list detailed in Table S9). Bulk pools were pressured for four consecutive days in a 5mL, 3% hematocrit culture in conditioned media (as mentioned above) supplemented with 10% (v/v) human serum (Interstate Blood Bank), starting at 1% total parasitemia. gDNA, used for library preparations and WGS, was harvested before (day 0) the 4-day QN selections (changing media every day with drug wash off after four days) at 0nM, 140nM, 180nM, 240nM, and after (day 4+) when there was enough genomic material to harvest (~2% parasitemia). The 0nM no drug control replicate well was set up at the same time as each drug selection, to ensure drug-specific killing of the pressured well and to harvest no-drug control gDNA at the same timepoint as its corresponding drug-pressured well. This no-drug control was used to account for allele frequency changes due to *in vitro* culture alone.

The gDNA from each time point was whole-genome sequenced and used for the QN bulk segregant analysis performed with the R package, QTLseqr[65]. As some gDNA bulks sequences exhibited low coverage compared to the progeny-clone based sequences, we used all 106,316 SNPs that distinguished the two parents. SNPs were then filtered using the filterSNPs function using the following restrictions: 0.1≤ reference allele frequency ≤0.9 to remove over- and under-represented SNPs in both bulks, (minimum total depth = 10)/ (maximum total depth = 200) and minimum sample depth = 5 to filter extremely low and high coverage SNPs in both bulks and in each bulk separately, respectively. SNPs were also removed if there was ≥100 read depth difference between bulks. QTLs were identified using the QTL-seq[102] and G'[103] approaches. A window size of 100kb was used (unless indicated otherwise for G' analysis) to calculate the tricube-smoothed Δ(SNP-*index*) and G statistic (or G') for each SNP within that widow. For the G' analysis, outlier regions were filtered based on Hampel's rule and QTLs were identified as regions with

False Discovery Rate (Benjamini-Hochberg-adjusted *p*-values or *q*-values) <0.01. For the Δ(SNP-*index*) analysis, QTLs were identified as regions that pass the 95% and 99% confidence intervals.

Progeny clone-based quantitative trait locus (QTL) mapping. The R package, R/qtl version 2[104] was used to map QTL peaks. To identify significant QTLs for each drug response phenotype, 1,000 permutations of phenotypic data (IC_{50}, IC_{90}) were performed to obtain a distribution of maximum log of the odds (LOD) scores. These LOD scores were then used to calculate the LOD threshold at 95% probability. Fine mapping of the QTL segments was performed using Bayesian interval mapping at a 95% confidence level.

CRISPR/Cas9 plasmid construction. The DMT1 (PF3D7_0715800) Y107N/S129L mutation or WT with binding-site mutations was introduced into the cross parents (NF54 JHU, Cam3.II G8) and five progeny (B-QN95-140-A5, B-CQ75-1-H9, B4-5, B5-4, Clow6, C-QN95-180-F8) using an all-in-one CRISPR/Cas9 plasmid (pDC2-co*Sp*Cas9-h*dhfr*[105]). The *P. falciparum* codon-optimized Cas9 endonuclease was derived from *Streptococcus pyogenes* and was expressed under a *calmodulin* promoter. The plasmid also carried a human dihydrofolate reductase (h*dhfr*) selectable marker (conferring resistance to the compound, WR99210) under a *P. chabaudi dhfr-ts* (*Pcdt*) promoter and a *U6* promoter for expressing the guide RNA (gRNA). The DMT1 WT and Y107N/S129L donors were synthesized in a pUC-GW-*amp* vector (Genewiz), with both donors also containing the same three silent (synonymous) mutations at the gRNA recognition site (referred to herein as binding-site mutations or bsmut) (prioritizing the PAM and/or the "seed" region <12nt upstream of the PAM) to prevent the donor or the edited recombinant locus from Cas9 endonuclease-mediated re-cleavage. The donors were PCR-amplified from the pUC-GW-*amp* vector and subcloned into the of pDC2-co*Sp*Cas9-h*dhfr* at the *Eco*RI and *Aat*II restriction sites by In-Fusion cloning. A gRNA was selected using ChopChop version 3[106] and Benchling (https://www.benchling.com), trying to be as close as possible to the mutation site, avoiding poly-T stretches of >3 Ts as they may cause premature transcription termination[107], and prioritizing gRNAs with low off-target scores and at least 3–4 mismatches to other sites in the genome that are preferably in the PAM and/or the "seed" region. Double-stranded gRNA blocks were synthesized as single-stranded DNA (Eurofins Genomics) and then phosphorylated, annealed, and cloned into the *Bbs*I restriction sites of pDC2-co*Sp*Cas9-h*dhfr* by T4 DNA ligase cloning.

To generate Cam3.II G8 parasites with WT (with bsmut) ThzK (PF3D7_1239600) (and N244/A301V mutant control with bsmut), FtsH1 (PF3D7_1239700) (and D695G mutant control with bsmut), and SAMC (PF3D7_1241600) (and I176K/S193A mutant control with bsmut), donors were synthesized in the pUC-GW-*amp* vector as described above with bsmuts for two gRNAs. The donors for ThzK and FtsH1 were subcloned into pDC2-co*Sp*Cas9-h*dhfr* as described above while the donor for SAMC was kept in the pUC-GW-*amp* vector due to difficulties with cloning. Two gRNAs were selected per gene and cloned into the *Bbs*I restriction sites to generate two separate plasmids per gene as described above.

To generate a PfNF54 DMT1 3' 3×human influenza hemagglutinin-based (HA) tagged parasite, a DMT1 donor with a homology region (HR) 1 (342bp), recodonized 3' end of DMT1 to disrupt homology with no stop codon (165bp), spacer (6bp), 3×HA tag with a stop codon, and 3' untranslated region (UTR) HR2 (509bp) was synthesized in a pUC-GW-*amp* vector (Genewiz), PCR amplified and cloned into the *Eco*RI/*Aat*II restriction sites of the pDC2-co*Sp*Cas9-h*dhfr* vector by In-Fusion cloning. Three gRNAs within the recodonized region were selected and cloned into the vector as described above.

To generate a *Pf*Cam3.II G8 DMT1 KO using CRISPR/Cas9 gene editing, 1202bp out of the 1305bp-long native PfDMT1 exon was replaced with a h*dhfr* cassette containing the *Pcdt* promoter, h*dhfr* WR99210-selectable marker, and 3' *hrp2* that was transcribed in the reverse orientation. The left homology (499bp) and right homology (437bp) regions were PCR amplified from Cam3.II G8 gDNA and inserted into the *Eco*RI/*Aat*II and *Apa*I restriction sites of the pDC2-co*Sp*Cas9-h*dhfr* vector, respectively, by In-Fusion cloning. Three gRNAs within the deleted region were selected and cloned into the vector as described above.

All final plasmids were purified using the NucleoBond Xtra Maxi kit (Macherey-Nagel) and confirmed by restriction digests and Sanger sequencing and are listed in Table S12. Primers used for cloning and verification are described in Table S11.

Parasite transfections. Asexual blood-stage parasites were electroporated with purified circular plasmid DNA as described[108]. Per transfection, a 2.5mL culture of 3% hematocrit, >5% ring-stage parasites was harvested and washed with 15 mL of 1× Cytomix[109]. 75μL of parasitized RBCs was then added to 50μg of plasmid DNA* and 1× Cytomix to a total volume of 440μL, transferred to a 0.2cm cuvette (Bio-Rad), and electroporated at a voltage of 0.31kV and capacitance of 950μF using a Gene-Pulser (Bio-Rad)[110]. *For SAMC SNP editing, 50μg each of pUC-GW with donor and CRISPR/Cas9 plasmid with one gRNA were co-transfected; for DMT1 KO, DMT1-3×HA, FtsH1 SNP, and ThzK SNP gene editing, 50μg each of CRISPR/Cas9 all-in-one plasmids contained the same donor but two distinct gRNA were co-transfected. Cells were transferred from the cuvette to a well in a 6-well plate containing 3% hematocrit blood+media mixture, and media was changed ~3–4h post-transfection (or sometimes ~15h later). Starting the day after the transfections, the cultures were maintained in 2.5nM WR99210 (if parasites have triple *dhfr* mutations; N51I/C59R/S108N) or 1nM WR99210 (if WT *dhfr*) for six consecutive days[111]. WR9210 was procured from Jacobus Pharmaceuticals. Successful gene editing was assessed via Sanger sequencing of PCR products amplified directly from bulk cultures or from bulk culture gDNA. DMT1-3×HA-tagged parasite clones were obtained by limiting dilution. Successful *dmt1*-3×HA tagging was confirmed via PCR, Sanger sequencing, immunofluorescence, and western blot assays. Successful *dmt1* KO was confirmed by PCR, Sanger sequencing, and gel electrophoresis. Oligonucleotide primers used in this study are listed in Table S11.

Western blot confirmation of DMT1-3×HA tagging. Western blots were performed with lysates from *Pf*NF54 DMT1-3×HA-tagged parasites and *Pf*NF54 PRELI-3×HA-tagged

parasites (positive control). Parasite cultures were washed twice in cold 1×PBS, and parasites were isolated by treatment with 0.05% saponin in PBS. Released parasites were lysed in 4% SDS, 0.5% Triton X-100 and 0.5% PBS supplemented with 1×protease inhibitors (Halt Protease and Phosphatase Inhibitor Cocktail, Thermo Scientific) and Pierce Universal Nuclease for Cell Lysis (Thermo Scientific). Samples were centrifuged at 14,000rpm for 10min to pellet cellular debris. 4×Laemmli Sample Buffer (Bio-Rad) was added to lysates and samples were denatured at 50°C for 15min (and not boiled to prevent the aggregation of the DMT1 transmembrane protein). Proteins were electrophoresed on precast 4–20% Tris-Glycine gels (Bio-Rad) and transferred onto nitrocellulose membranes. Western blots were probed with a 1:1000 dilution of primary antibodies to HA (mouse mAb; Cell Signaling), followed by a 1:5000 dilution of anti-mouse IgG H&L HRP-conjugated secondary antibodies (Abcam). Western blots were revealed using Pierce ECL Western Blotting Substrate (Thermo Scientific) and imaged on a ChemiDoc system (Bio-Rad).

Indirect immunofluorescence assays (IFAs). Harvested NF54 DMT1-3×HA-parasitized RBCs were washed twice in 1×PBS and fixed in methanol-free 4% v/v formaldehyde (Pierce), supplemented with 0.0075% v/v glutaraldehyde (Electron Microscopy Sciences) in 1×PBS for 30min at room temperature while stationary, followed by one 1×PBS wash. For mitochondria staining, harvested parasites were washed once with pre-warmed RPMI, stained with 50nM MitoTracker Red CMXRos (Invitrogen) at 37°C in the incubator while stationary prior to the 1×PBS wash and fixation, and were kept covered throughout. Cell membranes were then permeabilized in 0.1% Triton X-100 in 1×PBS for 30min at room temperature while stationary, followed by three 1×PBS washes. Autofluorescence was quenched using 0.1M glycine in 1×PBS for 15min at room temperature while rotating. Blocking was performed with 3% w/v bovine serum albumin (BSA) and 0.1% Tween 20 (v/v) in 1×PBS overnight at 4°C while rotating. Cells were incubated with primary antibodies for 2–4hrs at room temperature while rotating, with dilutions ranging from 1:50 to 1:200, followed by a 1h incubation with a species-specific fluorophore-conjugated secondary antibody diluted in 3% BSA and 0.1% Tween 20 in 1×PBS. As primary antibodies, we used rabbit anti-binding immunoglobin protein (BiP) (1:200) (kindly provided by Min Zhang), mouse anti-PfK13 (1:100) (clone E3[82]), rabbit anti-Rab11A, rat anti-Rab5B or -Rab7 (1:50) (kindly provided by Dr. Gordon Langsley), rabbit anti-PfACP (1:200) (kindly provided by Dr. Geoff McFadden), Nile Red (2.5μg/mL) (Invitrogen), rabbit anti-PfEXP2 (1:200) (MR4), mouse anti-PfCRT (1:200) (clone 2[112]), and rabbit anti-plasmepsin 2 (PM2) (1:100) (MR4). For organelle primary antibodies raised in rabbit, Alexa Fluor Plus 594-conjugated goat anti-rabbit IgG (H+L) secondary (1:3000) (Invitrogen) was used; for organelle mouse primary antibodies, Alexa Fluor 594-conjugated goat anti-mouse secondary (1:2000) (Invitrogen); for organelle rat primary antibodies, Alexa Fluor 594-conjugated goat anti-rat secondary (1:2000) (Invitrogen). Rat anti-HA (1:2000) (Millipore Sigma) and Alexa Fluor 488-conjugated goat anti-rat secondary (1:2000) (Invitrogen) were used to probe for DMT1-3×HA in co-stains with MitoTracker Red CMXRos, Nile Red, and organelle primary antibodies raised in mice or rabbits. Mouse anti-HA (1:100) (Cell Signaling) and Alexa Fluor 488-conjugated goat anti-

mouse secondary (1:1000) (Invitrogen) were used for probing for DMT1-3×HA in co-stains with organelle primary antibodies raised in rats.

Thin blood smears of stained RBCs were prepared on microscope slides and mounted with high-performance/high-tolerance cover slips (Zeiss) using ProLong Diamond Antifade Mountant with DAPI (Invitrogen) pre-warmed to room temperature. Mounted samples were cured overnight and were imaged using a Nikon TiE Eclipse inverted microscope with a Nikon A1 scanning confocal with a GaAsP spectral detector, and a CFI Plan Apochromat Lambda oil immersion objective with 100× magnification (1.45 numerical aperture). 0.2 μm step size Z-stacks were taken for each parasitized RBC. NIS-Elements version 5.02 (Nikon) was used to control the microscope and camera and crop images. Imaris version 9 (Oxford Instruments) was used to perform deconvolution using 5 (for DAPI) or 10 (for HA and organelle channels) iterations of the Richardson-Lucy algorithm for each image and quantify colocalization of the deconvolved Z-stacks using the Colocalization Module. Statistical analyses and visualization of the colocalization were performed with Prism version 10 (GraphPad). Fiji[113] version 2.11.0 (ImageJ) was used to adjust brightness and contrast, overlay channels, and prepare montages. For 3D rendering of the deconvolved images, the Imaris software was used.

β-hematin inhibition assays. A solution containing deionized H_2O/305.5mM NP-40 Surfact-Amps Detergent solution (ThermoFisher Scientific)/dimethyl-sulfoxide (DMSO) was prepared at a v/v ratio of 70%/20%/10%, respectively, and 100μL was added to columns 1–11 of a flat-bottomed 96-well plate. Working stocks of test and control compounds were constituted to 20mM (5mM for md-ADQ), from which 20μL (80μL for md-ADQ) of each was added to wells in duplicate in column 12 together with deionized H_2O (140μL; 80μL for md-ADQ) and 305.5mM NP-40 detergent (40μL). This effectively lowered the final drug concentration to 2mM. Each compound (100μL) was then serially diluted from columns 12 to 2 (column 1 served as a blank). A 25mM hematin stock solution was prepared by sonicating hemin (Sigma Life Sciences) in DMSO for 3min and 178.8μL of this solution was suspended in 20mL of acetate buffer (1M, pH 4.8) (made with sodium acetate (Sigma Aldrich) and acetic acid (Fisher Scientific)) and thoroughly mixed. The homogenous suspension (100μL) was then added to all wells to give a final 0.5M buffer and 100mM hematin concentration, as well as a 0.5mM drug concentration in column 12. Plates were covered and incubated at 37°C for 5 h after which 32μL of a 50% pyridine solution (20% (v/v) H_2O, 20% (v/v) acetone, 10% (v/v) 2M HEPES buffer (pH 7.4) and 50% (v/v) pyridine (Sigma Aldrich)) was added to each well. 60μL of acetone was then added to each well to assist with hematin dispersion. The UV-vis absorbance of each well was read at 405nm on a SpectraMax P340 plate reader. The β-hematin IC_{50} values for each compound were calculated from the absorbance values at 405nm using sigmoidal dose-response curve fitting analysis (Prism version 10, GraphPad).

Sequence alignment. The DMT1 protein sequence for the *P. falciparum* NF54 (PF3D7_0715800) strain and the orthologous DMT1 sequences from reference strains of *P. reichenowi* (PRCDC_0713100), *P. adleri* (PADL01_0713800), *P. gaboni* (PGSY75_0715800), *P. vivax* (PVP01_1424900), *P. knowlesi* (PKNH_1424800), *P. ovale* (PocGH01_14032100), *P. malariae* (PmUG01_14040800), *P. cynomolgi*

(PcyM_1426000), *P. chabaudi* (PCHAS_1423900), *P. berghei* (PBANKA_1422100), *P. yoelii* (PY17X_1424100), and *P. gallinaceum* (PGAL8A_00520500) were obtained from the PlasmoDB.org database[75]. Clustal Omega[114], which uses the HHalign algorithm, was used to perform multiple sequence alignments and generate phylogeny trees. EMBOSS Needle, which uses the Needleman-Wunsch algorithm, was used to perform global pairwise sequence alignments and calculate the percentage of positions in the alignment that are identical[115]. Both bioinformatic tools were accessed through EMBL-EBI[116].

DMT1 NF54 and Cam3.II protein expression and purification and QN, CQ transport measurements. The NF54 (QN- and CQ-sensitive) and Cam3.II (QN- and CQ-resistant) variants of the DMT1 and PfCRT proteins as well as Band 3 protein (anion transport control) were expressed, purified, and reconstituted in preformed liposomes as described previously[74], with some modifications. Uptake of [^{3}H]-CQ 300nM (1 Ci/mmol) or [^{3}H]-QN (300nM (1 Ci/mmol) was measured after diluting PfCRT, DMT1, or Band 3-containing proteoliposomes in 50 µl of 100 mM Tris/MES, pH 5.5 in the presence or absence of the indicated compounds. Band 3 was used as a negative control, for which we expected no or minimal CQ and QN uptake. The protein-specific uptake (pmol/mg) was determined by subtracting the time-dependent accumulation of the tested compounds in control liposomes (lacking PfCRT, DMT1 or Band 3) from the accumulation measured in proteoliposomes containing one of these proteins. Data were collected in three independent experiments, performed in duplicate, and are represented as the mean uptake ± SEM at each timepoint.

Acknowledgments

Funding for this work was kindly provided by the National Institute of Allergy and Infectious Diseases, National Institutes of Health (R37 AI050234 and R01 AI185559 to D.A.F.; R01 AI147628 to F.M., M.Q. and D.A.F.) and the Bill & Melinda Gates Foundation (OPP1201387 to D.A.F. and P.S.). M.K. gratefully acknowledges funding support from the Japan Student Services Organization and a scholarship from the New York Hideyo Noguchi Memorial Society. S.M. gratefully acknowledges funding support Human Frontiers Science Program Long-Term Fellowship (LT000976/2016-L) and the NIH (R01 AI182318). The IFA studies used the resources of the Herbert Irving Comprehensive Cancer Center Confocal and Specialized Microscopy Shared Resource, funded in part through NIH/NCI Cancer Center Support Grant P30CA013696, and with the assistance of Drs. Haojie Ji and Theresa Swayne.

References

1. World Health Organization. World malaria report 2023. 283 (2023).
2. Amato, R. *et al.* Origins of the current outbreak of multidrug-resistant malaria in southeast Asia: a retrospective genetic study. *Lancet Infect Dis* **18**, 337-345 (2018).
3. Ward, K.E., Fidock, D.A. & Bridgford, J.L. *Plasmodium falciparum* resistance to artemisinin-based combination therapies. *Curr Opin Microbiol* **69**, 102193 (2022).

4. Achan, J. *et al.* Quinine, an old anti-malarial drug in a modern world: role in the treatment of malaria. *Malar J* **10**, 144 (2011).
5. A, N. Formação de raça do hematozoario do impaludismo resistente a quinina. *Mem Inst Oswaldo Cruz* **2**, 131-40 (1910).
6. M, C. Les injections endo-veineuses du bleu de méthylène dans le paludisme. *Bull Soc Pathol Exot* **1**, 292-5 (1908).
7. Rodriguez-Valero, N. *et al.* Suspected quinine resistant *P. falciparum* severe malaria possibly acquired in Ivory Coast. *Parasitol Int* **67**, 684-687 (2018).
8. Oboh, M.A. *et al.* Multiple *Plasmodium falciparum* drug resistance polymorphisms identified in a pregnant woman with severe malaria and a concomitant spontaneous abortion in Cross River, Nigeria, West Africa. *Malar J* **21**, 160 (2022).
9. Bertaux, L. *et al.* Quinine-resistant malaria in traveler returning from French Guiana, 2010. *Emerg Infect Dis* **17**, 943-5 (2011).
10. Demar, M. & Carme, B. *Plasmodium falciparum in vivo* resistance to quinine: description of two RIII responses in French Guiana. *Am J Trop Med Hyg* **70**, 125-7 (2004).
11. Legrand, E., Volney, B., Meynard, J.B., Mercereau-Puijalon, O. & Esterre, P. *In vitro* monitoring of *Plasmodium falciparum* drug resistance in French Guiana: a synopsis of continuous assessment from 1994 to 2005. *Antimicrob Agents Chemother* **52**, 288-98 (2008).
12. Huttinger, F. *et al.* Sensitivity to artemisinin, mefloquine and quinine of *Plasmodium falciparum* in northwestern Thailand. *Wien Klin Wochenschr* **122 Suppl 3**, 52-6 (2010).
13. Pradines, B. *et al.* Quinine-resistant malaria in traveler returning from Senegal, 2007. *Emerg Infect Dis* **16**, 546-8 (2010).
14. Mayxay, M. *et al. In vitro* antimalarial drug susceptibility and *pfcrt* mutation among fresh *Plasmodium falciparum* isolates from the Lao PDR (Laos). *Am J Trop Med Hyg* **76**, 245-50 (2007).
15. Ringwald, P., Bickii, J. & Basco, L.K. *In vitro* activity of dihydroartemisinin against clinical isolates of *Plasmodium falciparum* in Yaounde, Cameroon. *Am J Trop Med Hyg* **61**, 187-92 (1999).
16. Mutanda, L.N. Assessment of drug resistance to the malaria parasite in residents of Kampala, Uganda. *East Afr Med J* **76**, 421-4 (1999).
17. Pradines, B. *et al. In vitro* susceptibility of Gabonese wild isolates of *Plasmodium falciparum* to artemether, and comparison with chloroquine, quinine, halofantrine and amodiaquine. *Parasitology* **117 (Pt 6)**, 541-5 (1998).
18. Ferdig, M.T. *et al.* Dissecting the loci of low-level quinine resistance in malaria parasites. *Mol Microbiol* **52**, 985-97 (2004).
19. Sanchez, C.P. *et al.* A HECT ubiquitin-protein ligase as a novel candidate gene for altered quinine and quinidine responses in *Plasmodium falciparum*. *PLoS Genet* **10**, e1004382 (2014).
20. Nkrumah, L.J. *et al.* Probing the multifactorial basis of *Plasmodium falciparum* quinine resistance: evidence for a strain-specific contribution of the sodium-proton exchanger PfNHE. *Mol Biochem Parasitol* **165**, 122-31 (2009).

21. Dziekan, J.M. *et al.* Cellular thermal shift assay for the identification of drug-target interactions in the *Plasmodium falciparum* proteome. *Nat Protoc* **15**, 1881-1921 (2020).
22. Cowman, A.F., Galatis, D. & Thompson, J.K. Selection for mefloquine resistance in *Plasmodium falciparum* is linked to amplification of the *pfmdr1* gene and cross-resistance to halofantrine and quinine. *Proc Natl Acad Sci U S A* **91**, 1143-7 (1994).
23. Reed, M.B., Saliba, K.J., Caruana, S.R., Kirk, K. & Cowman, A.F. Pgh1 modulates sensitivity and resistance to multiple antimalarials in *Plasmodium falciparum*. *Nature* **403**, 906-909 (2000).
24. Foley, M. & Tilley, L. Quinoline antimalarials: mechanisms of action and resistance and prospects for new agents. *Pharmacol Ther* **79**, 55-87 (1998).
25. Ehrlich, H.Y., Jones, J. & Parikh, S. Molecular surveillance of antimalarial partner drug resistance in sub-Saharan Africa: a spatial-temporal evidence mapping study. *Lancet Microbe* **1**, e209-e217 (2020).
26. Asua, V. *et al.* Changing pevalence of potential mediators of aminoquinoline, antifolate, and artemisinin resistance across Uganda. *J Infect Dis* **223**, 985-994 (2021).
27. Ecker, A., Lehane, A.M., Clain, J. & Fidock, D.A. PfCRT and its role in antimalarial drug resistance. *Trends Parasitol* **28**, 504-14 (2012).
28. Sa, J.M. *et al.* Geographic patterns of *Plasmodium falciparum* drug resistance distinguished by differential responses to amodiaquine and chloroquine. *Proc Natl Acad Sci U S A* **106**, 18883-18889 (2009).
29. Veiga, M.I. *et al.* Globally prevalent PfMDR1 mutations modulate *Plasmodium falciparum* susceptibility to artemisinin-based combination therapies. *Nat Commun* **7**, 11553 (2016).
30. Patel, J.J. *et al.* Chloroquine susceptibility and reversibility in a *Plasmodium falciparum* genetic cross. *Mol Microbiol* **78**, 770-87 (2010).
31. Wellems, T.E. & Plowe, C.V. Chloroquine-resistant malaria. *J Infect Dis* **184**, 770-6 (2001).
32. Tinto, H. *et al.* Relationship between the *pfcrt* T76 and the *pfmdr-1* Y86 mutations in *Plasmodium falciparum* and *in vitro*/*in vivo* chloroquine resistance in Burkina Faso, West Africa. *Infect Genet Evol* **3**, 287-92 (2003).
33. Mu, J. *et al.* Multiple transporters associated with malaria parasite responses to chloroquine and quinine. *Mol Microbiol* **49**, 977-989 (2003).
34. Sidhu, A.B., Verdier-Pinard, D. & Fidock, D.A. Chloroquine resistance in *Plasmodium falciparum* malaria parasites conferred by *pfcrt* mutations. *Science* **298**, 210-213 (2002).
35. Tyagi, R.K. *et al.* High-level artemisinin-resistance with quinine co-resistance emerges in *P. falciparum* malaria under *in vivo* artesunate pressure. *BMC Med* **16**, 181 (2018).
36. Wang, P., Read, M., Sims, P.F. & Hyde, J.E. Sulfadoxine resistance in the human malaria parasite *Plasmodium falciparum* is determined by mutations in dihydropteroate synthetase and an additional factor associated with folate utilization. *Mol Microbiol* **23**, 979-86 (1997).
37. Cowman, A.F., Morry, M.J., Biggs, B.A., Cross, G.A. & Foote, S.J. Amino acid changes linked to pyrimethamine resistance in the dihydrofolate reductase-

thymidylate synthase gene of *Plasmodium falciparum*. *Proc Natl Acad Sci U S A* **85**, 9109-13 (1988).

38. Wellems, T.E., Walker-Jonah, A. & Panton, L.J. Genetic mapping of the chloroquine-resistance locus on *Plasmodium falciparum* chromosome 7. *Proc Natl Acad Sci U S A* **88**, 3382-6 (1991).
39. Su, X.Z., Kirkman, L.A., Fujioka, H. & Wellems, T.E. Complex polymorphisms in an approximately 330 kDa protein are linked to chloroquine-resistant *P. falciparum* in Southeast Asia and Africa. *Cell* **91**, 593-603 (1997).
40. Fidock, D.A. *et al.* Mutations in the *P. falciparum* digestive vacuole transmembrane protein PfCRT and evidence for their role in chloroquine resistance. *Mol Cell* **6**, 861-871 (2000).
41. Brenneman, K.V. *et al.* Optimizing bulk segregant analysis of drug resistance using *Plasmodium falciparum* genetic crosses conducted in humanized mice. *iScience* **25**, 104095 (2022).
42. Li, X. *et al.* Genetic mapping of fitness determinants across the malaria parasite *Plasmodium falciparum* life cycle. *PLoS Genet* **15**, e1008453 (2019).
43. Wellems, T.E. *et al.* A histidine-rich protein gene marks a linkage group favored strongly in a genetic cross of *Plasmodium falciparum*. *Cell* **49**, 633-42 (1987).
44. Wellems, T.E. *et al.* Chloroquine resistance not linked to *mdr*-like genes in a *Plasmodium falciparum* cross. *Nature* **345**, 253-255 (1990).
45. Hayton, K. *et al.* Erythrocyte binding protein PfRH5 polymorphisms determine species-specific pathways of *Plasmodium falciparum* invasion. *Cell Host Microbe* **4**, 40-51 (2008).
46. Sa, J.M. *et al.* Artemisinin resistance phenotypes and K13 inheritance in a *Plasmodium falciparum* cross and *Aotus* model. *Proc Natl Acad Sci U S A* **115**, 12513-12518 (2018).
47. Vaughan, A.M. *et al. Plasmodium falciparum* genetic crosses in a humanized mouse model. *Nat Methods* **12**, 631-3 (2015).
48. Azuma, H. *et al.* Robust expansion of human hepatocytes in *Fah*$^{-/-}$/*Rag2*$^{-/-}$/*Il2rg*$^{-/-}$ mice. *Nat Biotechnol* **25**, 903-10 (2007).
49. Combrinck, J.M. *et al.* Insights into the role of heme in the mechanism of action of antimalarials. *ACS Chem Biol* **8**, 133-7 (2013).
50. Slater, A.F. & Cerami, A. Inhibition by chloroquine of a novel haem polymerase enzyme activity in malaria trophozoites. *Nature* **355**, 167-9 (1992).
51. Ncokazi, K.K. & Egan, T.J. A colorimetric high-throughput beta-hematin inhibition screening assay for use in the search for antimalarial compounds. *Anal Biochem* **338**, 306-19 (2005).
52. Carter, M.D., Phelan, V.V., Sandlin, R.D., Bachmann, B.O. & Wright, D.W. Lipophilic mediated assays for beta-hematin inhibitors. *Comb Chem High Throughput Screen* **13**, 285-92 (2010).
53. Sandlin, R.D. *et al.* Use of the NP-40 detergent-mediated assay in discovery of inhibitors of beta-hematin crystallization. *Antimicrob Agents Chemother* **55**, 3363-9 (2011).
54. Olafson, K.N., Nguyen, T.Q., Rimer, J.D. & Vekilov, P.G. Antimalarials inhibit hematin crystallization by unique drug-surface site interactions. *Proc Natl Acad Sci U S A* **114**, 7531-7536 (2017).

55. Uwimana, A. *et al.* Emergence and clonal expansion of *in vitro* artemisinin-resistant *Plasmodium falciparum kelch13* R561H mutant parasites in Rwanda. *Nat Med* **26**, 1602-1608 (2020).
56. Amaratunga, C. *et al.* Artemisinin-resistant *Plasmodium falciparum* in Pursat province, western Cambodia: a parasite clearance rate study. *Lancet Infect Dis* **12**, 851-8 (2012).
57. Straimer, J. *et al.* K13-propeller mutations confer artemisinin resistance in *Plasmodium falciparum* clinical isolates. *Science* **347**, 428-431 (2015).
58. Lee, A.H., Symington, L.S. & Fidock, D.A. DNA repair mechanisms and their biological roles in the malaria parasite *Plasmodium falciparum*. *Microbiol Mol Biol Rev* **78**, 469-486 (2014).
59. Creasey, A. *et al.* Maternal inheritance of extrachromosomal DNA in malaria parasites. *Mol Biochem Parasitol* **65**, 95-8 (1994).
60. Okamoto, N., Spurck, T.P., Goodman, C.D. & McFadden, G.I. Apicoplast and mitochondrion in gametocytogenesis of *Plasmodium falciparum*. *Eukaryot Cell* **8**, 128-32 (2009).
61. Preston, M.D. *et al.* A barcode of organellar genome polymorphisms identifies the geographic origin of *Plasmodium falciparum* strains. *Nat Commun* **5**, 4052 (2014).
62. Vaidya, A.B., Morrisey, J., Plowe, C.V., Kaslow, D.C. & Wellems, T.E. Unidirectional dominance of cytoplasmic inheritance in two genetic crosses of *Plasmodium falciparum*. *Mol Cell Biol* **13**, 7349-57 (1993).
63. Creasey, A.M. *et al.* Uniparental inheritance of the mitochondrial gene *cytochrome b* in *Plasmodium falciparum*. *Curr Genet* **23**, 360-4 (1993).
64. Button-Simons, K.A. *et al.* The power and promise of genetic mapping from *Plasmodium falciparum* crosses utilizing human liver-chimeric mice. *Commun Biol* **4**, 734 (2021).
65. Mansfeld, B.N. & Grumet, R. QTLseqr: an R package for bulk segregant analysis with next-generation sequencing. *Plant Genome* **11**(2018).
66. Lopez-Barragan, M.J. *et al.* Directional gene expression and antisense transcripts in sexual and asexual stages of *Plasmodium falciparum*. *BMC Genomics* **12**, 587 (2011).
67. Cowell, A.N. *et al.* Mapping the malaria parasite druggable genome by using *in vitro* evolution and chemogenomics. *Science* **359**, 191-199 (2018).
68. Amberg-Johnson, K. *et al.* Small molecule inhibition of apicomplexan FtsH1 disrupts plastid biogenesis in human pathogens. *Elife* **6**(2017).
69. Goodman, C.D., Uddin, T., Spillman, N.J. & McFadden, G.I. A single point mutation in the *Plasmodium falciparum* FtsH1 metalloprotease confers actinonin resistance. *Elife* **9**(2020).
70. Tanveer, A. *et al.* An FtsH protease is recruited to the mitochondrion of *Plasmodium falciparum*. *PLoS One* **8**, e74408 (2013).
71. Krogh, A., Larsson, B., von Heijne, G. & Sonnhammer, E.L. Predicting transmembrane protein topology with a hidden Markov model: application to complete genomes. *J Mol Biol* **305**, 567-80 (2001).
72. Hoffman, K. & Stoffel, W. TMbase-a database of membrane spanning proteins segments. *Biochim Biophys Acta* **815**, 468-476 (1993).

73. Jumper, J. *et al.* Highly accurate protein structure prediction with AlphaFold. *Nature* **596**, 583-589 (2021).
74. Kim, J. *et al.* Structure and drug resistance of the *Plasmodium falciparum* transporter PfCRT. *Nature* **576**, 315-320 (2019).
75. Amos, B. *et al.* VEuPathDB: the eukaryotic pathogen, vector and host bioinformatics resource center. *Nucleic Acids Res* **50**, D898-D911 (2022).
76. Liu, W. *et al.* Origin of the human malaria parasite *Plasmodium falciparum* in gorillas. *Nature* **467**, 420-5 (2010).
77. Zhang, M. *et al.* Uncovering the essential genes of the human malaria parasite *Plasmodium falciparum* by saturation mutagenesis. *Science* **360**, eaap7847 (2018).
78. Bushell, E. *et al.* Functional profiling of a *Plasmodium* genome reveals an abundance of essential genes. *Cell* **170**, 260-272 e8 (2017).
79. Sayers, C.P., Mollard, V., Buchanan, H.D., McFadden, G.I. & Goodman, C.D. A genetic screen in rodent malaria parasites identifies five new apicoplast putative membrane transporters, one of which is essential in human malaria parasites. *Cell Microbiol* **20**(2018).
80. Kenthirapalan, S., Waters, A.P., Matuschewski, K. & Kooij, T.W. Functional profiles of orphan membrane transporters in the life cycle of the malaria parasite. *Nat Commun* **7**, 10519 (2016).
81. Birnbaum, J. *et al.* A Kelch13-defined endocytosis pathway mediates artemisinin resistance in malaria parasites. *Science* **367**, 51-59 (2020).
82. Gnadig, N.F. *et al.* Insights into the intracellular localization, protein associations and artemisinin resistance properties of *Plasmodium falciparum* K13. *PLoS Pathog* **16**, e1008482 (2020).
83. Yang, T. *et al.* Decreased K13 abundance reduces hemoglobin catabolism and proteotoxic stress, underpinning artemisinin resistance. *Cell Rep* **29**, 2917-2928 e5 (2019).
84. Palacpac, N.M. *et al.* Developmental-stage-specific triacylglycerol biosynthesis, degradation and trafficking as lipid bodies in *Plasmodium falciparum*-infected erythrocytes. *J Cell Sci* **117**, 1469-80 (2004).
85. Jackson, K.E. *et al.* Food vacuole-associated lipid bodies and heterogeneous lipid environments in the malaria parasite, *Plasmodium falciparum*. *Mol Microbiol* **54**, 109-22 (2004).
86. Hartwig, C.L. *et al.* Accumulation of artemisinin trioxane derivatives within neutral lipids of *Plasmodium falciparum* malaria parasites is endoperoxide-dependent. *Biochem Pharmacol* **77**, 322-36 (2009).
87. Waller, K.L. *et al.* Chloroquine resistance modulated *in vitro* by expression levels of the *Plasmodium falciparum* chloroquine resistance transporter. *J Biol Chem* **278**, 33593-601 (2003).
88. Sanchez, C.P. *et al.* The knock-down of the chloroquine resistance transporter PfCRT is linked to oligopeptide handling in *Plasmodium falciparum*. *Microbiol Spectr* **10**, e0110122 (2022).
89. Davidson, M.W., Griggs, B.G., Boykin, D.W. & Wilson, W.D. Molecular structural effects involved in the interaction of quinolinemethanolamines with DNA. Implications for antimalarial action. *J Med Chem* **20**, 1117-22 (1977).

90. Wong, W. *et al.* Mefloquine targets the *Plasmodium falciparum* 80S ribosome to inhibit protein synthesis. *Nat Microbiol* **2**, 17031 (2017).
91. Sheridan, C.M., Garcia, V.E., Ahyong, V. & DeRisi, J.L. The *Plasmodium falciparum* cytoplasmic translation apparatus: a promising therapeutic target not yet exploited by clinically approved anti-malarials. *Malar J* **17**, 465 (2018).
92. Bendrat, K., Berger, B.J. & Cerami, A. Haem polymerization in malaria. *Nature* **378**, 138-9 (1995).
93. Wicht, K.J., Mok, S. & Fidock, D.A. Molecular Mechanisms of Drug Resistance in *Plasmodium falciparum* Malaria. *Annu Rev Microbiol* **74**, 431-454 (2020).
94. Maiga, B. *et al.* Characteristics of severe malaria in children from 0 to 5 years at the hospital of Sikasso in Mali. *Mali Med* **34**, 1-5 (2019).
95. Tripathi, A.K., Mlambo, G., Kanatani, S., Sinnis, P. & Dimopoulos, G. *Plasmodium falciparum* gametocyte culture and mosquito infection through artificial membrane feeding. *J Vis Exp* (2020).
96. Li, H. & Durbin, R. Fast and accurate short read alignment with Burrows-Wheeler transform. *Bioinformatics* **25**, 1754-60 (2009).
97. Cingolani, P. *et al.* A program for annotating and predicting the effects of single nucleotide polymorphisms, SnpEff: SNPs in the genome of *Drosophila melanogaster* strain w^{1118}; *iso-2*; *iso-3*. *Fly (Austin)* **6**, 80-92 (2012).
98. Kanai, M. *et al.* Comparative analysis of *Plasmodium falciparum* genotyping via SNP detection, microsatellite profiling, and whole-genome sequencing. *Antimicrob Agents Chemother* **66**, e0116321 (2022).
99. Li, H. *et al.* The sequence alignment/map format and SAMtools. *Bioinformatics* **25**, 2078-2079 (2009).
100. de Hoon, M.J., Imoto, S., Nolan, J. & Miyano, S. Open source clustering software. *Bioinformatics* **20**, 1453-1454 (2004).
101. Saldanha, A.J. Java Treeview--extensible visualization of microarray data. *Bioinformatics* **20**, 3246-3248 (2004).
102. Takagi, H. *et al.* QTL-seq: rapid mapping of quantitative trait loci in rice by whole genome resequencing of DNA from two bulked populations. *Plant J* **74**, 174-83 (2013).
103. Magwene, P.M., Willis, J.H. & Kelly, J.K. The statistics of bulk segregant analysis using next generation sequencing. *PLoS Comput Biol* **7**, e1002255 (2011).
104. Broman, K.W., Wu, H., Sen, S. & Churchill, G.A. R/qtl: QTL mapping in experimental crosses. *Bioinformatics* **19**, 889-90 (2003).
105. Adjalley, S. & Lee, M.C.S. CRISPR/Cas9 editing of the *Plasmodium falciparum* genome. *Methods Mol Biol* **2470**, 221-239 (2022).
106. Labun, K. *et al.* CHOPCHOP v3: expanding the CRISPR web toolbox beyond genome editing. *Nucleic Acids Res* **47**, W171-W174 (2019).
107. Roy, K.R. *et al.* Multiplexed precision genome editing with trackable genomic barcodes in yeast. *Nat Biotechnol* **36**, 512-520 (2018).
108. Fidock, D.A., Nomura, T. & Wellems, T.E. Cycloguanil and its parent compound proguanil demonstrate distinct activities against *Plasmodium falciparum* malaria parasites transformed with human dihydrofolate reductase. *Mol Pharmacol* **54**, 1140-7 (1998).

109. McLean, A., Newell, D. & Baker, G. The metabolism of chlorambucil. *Biochem Pharmacol* **25**, 2331-5 (1976).
110. Adjalley, S.H., Lee, M.C. & Fidock, D.A. A method for rapid genetic integration into *Plasmodium falciparum* utilizing mycobacteriophage Bxb1 integrase. *Methods Mol Biol* **634**, 87-100 (2010).
111. Fidock, D.A. & Wellems, T.E. Transformation with human *dihydrofolate reductase* renders malaria parasites insensitive to WR99210 but does not affect the intrinsic activity of proguanil. *Proc Natl Acad Sci U S A* **94**, 10931-6 (1997).
112. Murithi, J.M. *et al.* The *Plasmodium falciparum* ABC transporter ABCI3 confers parasite strain-dependent pleiotropic antimalarial drug resistance. *Cell Chem Biol* **29**, 824-839 e6 (2022).
113. Schindelin, J. *et al.* Fiji: an open-source platform for biological-image analysis. *Nat Methods* **9**, 676-82 (2012).
114. Sievers, F. *et al.* Fast, scalable generation of high-quality protein multiple sequence alignments using Clustal Omega. *Mol Syst Biol* **7**, 539 (2011).
115. Needleman, S.B. & Wunsch, C.D. A general method applicable to the search for similarities in the amino acid sequence of two proteins. *J Mol Biol* **48**, 443-53 (1970).
116. Madeira, F. *et al.* Search and sequence analysis tools services from EMBL-EBI in 2022. *Nucleic Acids Res* **50**, W276-W279 (2022).

Figures

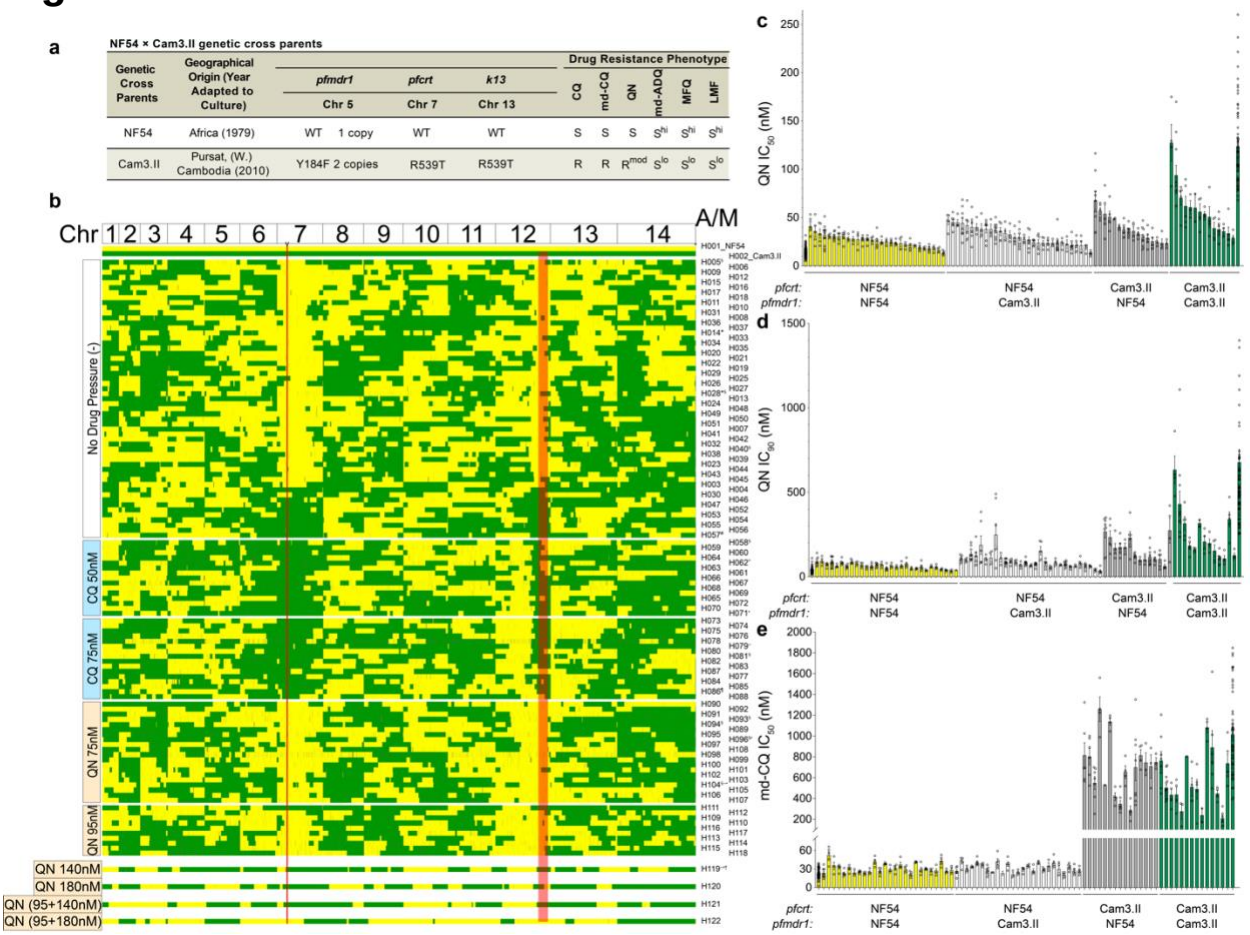

Fig. 1: A *P. falciparum* NF54×Cam3.II genetic cross yielded 120 independent recombinant progeny with diverse genomic and drug resistance profiles.

a, NF54×Cam3.II genetic cross parent information. [a]Dd2 PfCRT haplotype: M74I/N75E/K76T/A220S/Q271E/N326S/I356T/R371I. *k13*: *kelch-13* (PF3D7_1343700); *pfcrt*: *chloroquine resistance transporter* (PF3D7_0709000); *pfmdr1*: *multidrug resistance protein 1* (PF3D7_0523000). ADQ: amodiaquine; ART: artemisinin; CQ: chloroquine; LMF: lumefantrine; md-ADQ: mono-desethyl amodiaquine; md-CQ: monodesethyl-chloroquine; MFQ: mefloquine; md-CQ: monodesethyl-chloroquine; PPQ: piperaquine; QN: quinine. R, resistant; R^{mod}, moderate resistance; S, sensitive; S^{hi}, high sensitivity; S^{lo}, low sensitivity. **b**, Representative progeny recombinant clones per haplotype are hierarchically clustered by similarity based on their NF54 (yellow) or Cam3.II (green) alleles at 13,116 SNP positions within each selection condition: no drug pressure, chloroquine (CQ) 50nM or 75nM, or quinine (QN) 75nM, 95nM, 140nM, 180nM, (95nM+140nM), (95nM+180nM), or (95nM+140nM+240nM), in that order. If a haplotype was obtained in more than one selection condition, the genotypes are only shown once and the selection conditions they also appear in are listed on the right. H, haplotype; A/M, apicoplast/mitochondria; red line, *pfcrt*; red box, chromosome 12 QTL locus. **c**,**d**, QN response as measured by mean IC_{50} (**c**) and IC_{90} (**d**) values ± SEM. **e**, monodesethyl-Chloroquine response as measured by mean IC_{50} values ± SEM. (N,n=1–85,2). md-CQ, monodesethyl-Chloroquine; QN, quinine.

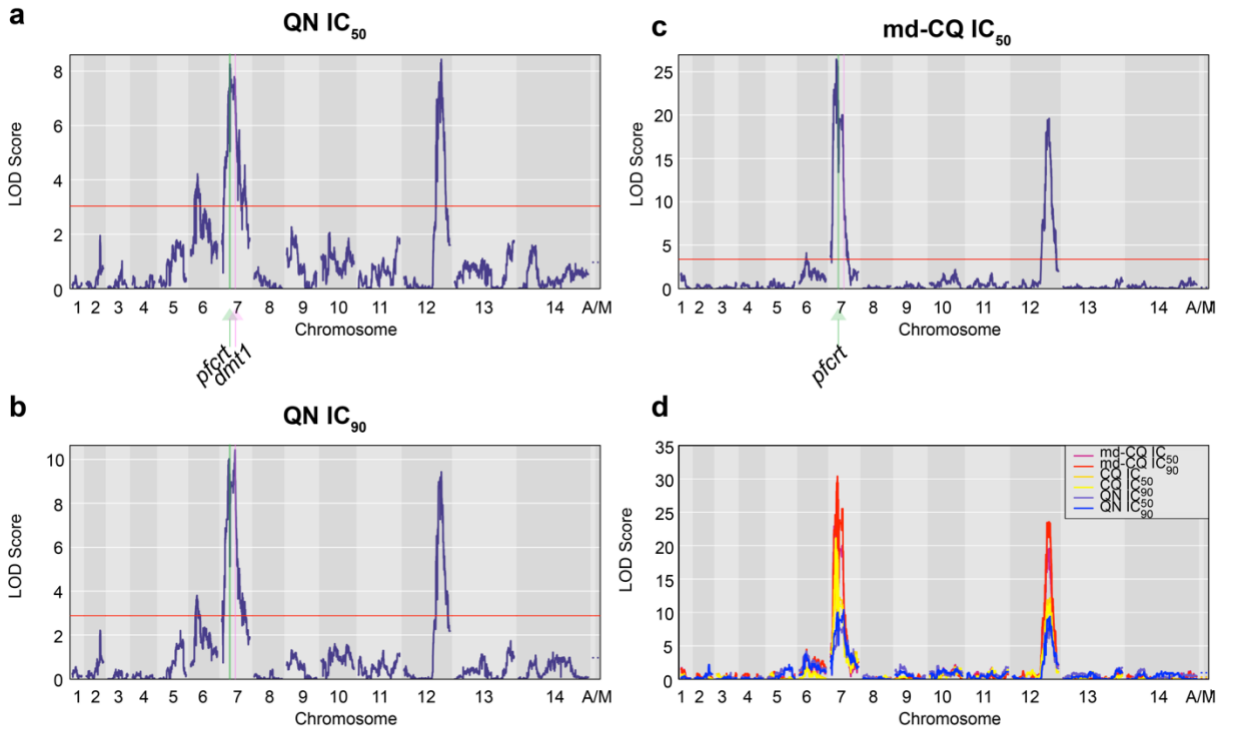

e

List of significant QTL segments identified by progeny clone-based analyses.

Drug response phenotypes	Chromosome	Position	LOD Score	Start position	End position	Size (bp)	% variance	Genes of interest
QN IC_{50}	6	387,269	4.21	242,806	967,817	725,011	19.0%	
QN IC_{50}	7	468,471	8.25	392,420	719,023	326,603	33.8%	*dmt1 + pfcrt*
QN IC_{50}	12	1,780,135	8.43	1,564,694	1,846,858	282,164	34.4%	*thzk + ftsh1 + samc*
QN IC_{90}	6	362,644	3.80	255,008	967,817	712,809	18.2%	
QN IC_{90}	7	701,206	10.42	379,842	717,936	338,094	42.4%	*dmt1 + pfcrt*
QN IC_{90}	12	1,780,135	9.43	1,644,803	1,791,218	146,415	39.3%	*thzk + ftsh1 + samc*
md-CQ IC_{50}	6	404,679	4.12	242,806	1,163,974	921,168	20.6%	
md-CQ IC_{50}	7	369,222	26.41	369,222	434,294	65,072	77.3%	*pfcrt*
md-CQ IC_{50}	12	1,746,445	19.60	1,666,819	1,749,151	82,332	66.7%	
md-CQ IC_{90}	6	404,679	4.50	281,586	1,211,193	929,607	23.0%	
md-CQ IC_{90}	7	414,358	30.40	383,125	435,497	52,372	83.0%	*pfcrt*
md-CQ IC_{90}	12	1,732,975	23.58	1,644,803	1,791,218	146,415	74.7%	*thzk + ftsh1 + samc*
CQ IC_{50}	7	414,358	19.10	379,842	433,609	53,767	81.6%	*pfcrt*
CQ IC_{50}	12	1,770,830	12.16	1,644,803	1,791,218	146,415	66.0%	*thzk + ftsh1 + samc*
CQ IC_{90}	7	342,797	21.17	313,716	373,413	59,697	84.7%	
CQ IC_{90}	12	1,770,830	11.27	1,644,803	1,791,218	146,415	63.2%	*thzk + ftsh1 + samc*

Fig. 2: QTL mapping of QN, CQ, and md-CQ progeny reveals a non-*pfcrt*-centered chr 7 QN IC_{90} peak and additional loci that overlap on chr 6 and chr 12.

a-**c**, LOD plots for mean QN IC_{50} (**a**), QN IC_{90} (**b**), and md-CQ IC_{50} (**c**) values. The red line indicates the 95% probability threshold. **d**, md-CQ, CQ, and QN LOD plots overlaid. QTL, quantitative trait locus; LOD, log of the odds; md-CQ, monodesethyl-Chloroquine; CQ, chloroquine; QN, quinine; IC_{50}, 50% growth inhibitory concentration; IC_{90}, 90% growth inhibitory concentration. **e**, List of significant QTL segments identified by progeny clone-based analysis. chr 7: *chloroquine resistance transporter* (*pfcrt*; PF3D7_0709000) (402,385..406,341) (green line), *drug/metabolite transporter* (putative) (*dmt1*; PF3D7_0715800) (695,091 - 697,180) (pink line). chr 12: *hydroxyethylthiazole kinase* (*thzk*; PF3D7_1239600) (1,652,687..1,654,402), *ATP-dependent zinc metalloprotease* (*ftsh1*; PF3D7_1239700) (1,654,438..1,658,821), *S-adenosylmethionine mitochondrial carrier protein* (*samc*; PF3D7_1241600) (1,774,021..1,776,962).

a Top candidate genes from progeny clone-based QN, CQ, and md-CQ QTL analyses

QTL	Gene Name	Gene Location	SNPs between NF54, Cam3.II	Mutable in *P. falciparum*[77]	*P. falciparum* mutant fitness[77]	*P. berghei* KO (PlasmoGEM)[78]	Association with antiplasmodial resistance
QN chr 7	drug metabolite transporter 1 (*dmt1*), putative	Pf3D7_07_v3:695,091..697,180(-)	Y107N/S129L/N155	Yes	-3.1	Dispensable	
QN, CQ md-CQ chr 12	S-adenosylmethionine mitochondrial carrier protein (*samc*), putative	Pf3D7_12_v3:1,774,021..1,776,962(+)	I176K/S193A	No	-3.3	Essential	MMV019662, MMV028038 selected for CNVs[67]
	ATP-dependent zinc metalloprotease (*ftsh1*)	Pf3D7_12_v3:1,654,438..1,658,821(+)	D695G	Yes	-1.0	ND	G489C confers actinonin^{R} [69]
	hydroxyethylthiazole kinase (*thzk*)	Pf3D7_12_v3:1,652,687..1,654,402(-)	N244/A301V	Yes	-2.2	N/A	

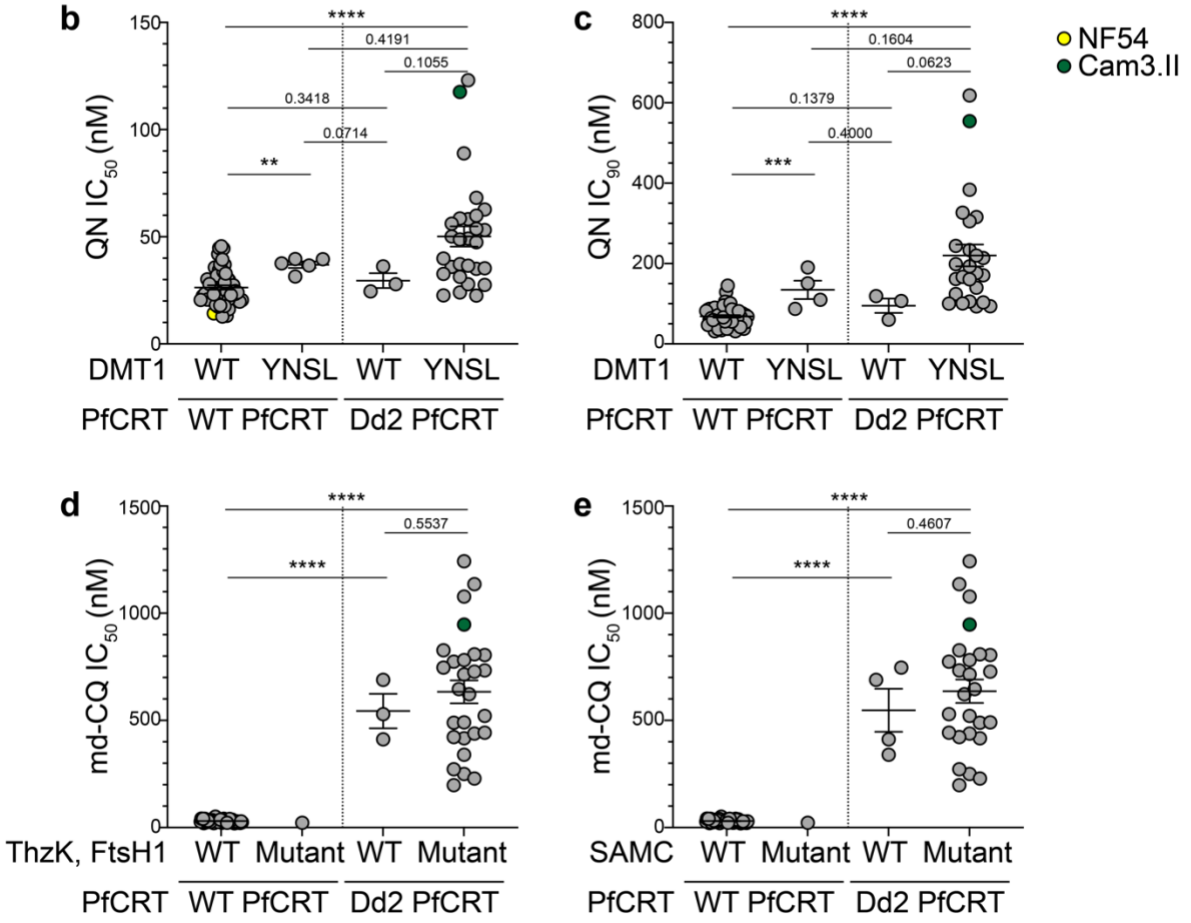

Fig. 3: Identification of the top candidate genes from the QN chr 7 and QN, CQ, md-CQ chr 12 QTL peaks.

a, Top candidate genes from progeny clone-based QN, CQ, and md-CQ QTL analyses. QTL, quantitative trait locus; SNP, single-nucleotide polymorphism; QN, quinine; CQ, chloroquine; md, monodesethyl; CDS, coding sequence; KO, knockout; CNV, copy number variants; ND, not determined; N/A, not applicable. [77]: the closer the mutant fitness score is to -4, the gene is predicted to have a higher fitness cost. [78]: essentiality of gene orthologs in *P. berghei*: PBANKA_142210, PBANKA_1455000, PBANKA_1454100. [67]Cowell, A.N. *et al Science* (2018): MMV028038 also selected for CNVs in PF3D7_0109800 and PF3D7_0108400, and SNPs in PF3D7_0107500 (M398I/A1208E), PF3D7_0400100 (R269S/E270A/E270D), PF3D7_1028300 (H169N), PF3D7_1354900 (N370I), PF3D7_1414700 (A684T); MMV019662 for CNVs in PF3D7_0108400. [69]Goodman, C.D. *et al eLife* (2020). All genes are expressed in the *P. falciparum* asexual blood stages according to López-Barragán, M.J. *et al BMC Genomics* (2011). **b**-**e**, QN (**b**,**c**) and md-CQ (**d**,**e**) IC levels for the profiled unedited cross progeny and two parents, grouped by *pfcrt*, *dmt1*, *thzk*, *ftsh1*, and *samc* genotypes. Statistical significance was determined by Mann-Whitney *U* tests (N,n=1–27,2). ***p* < 0.01, ****p* < 0.001, ****p* < 0.0001.

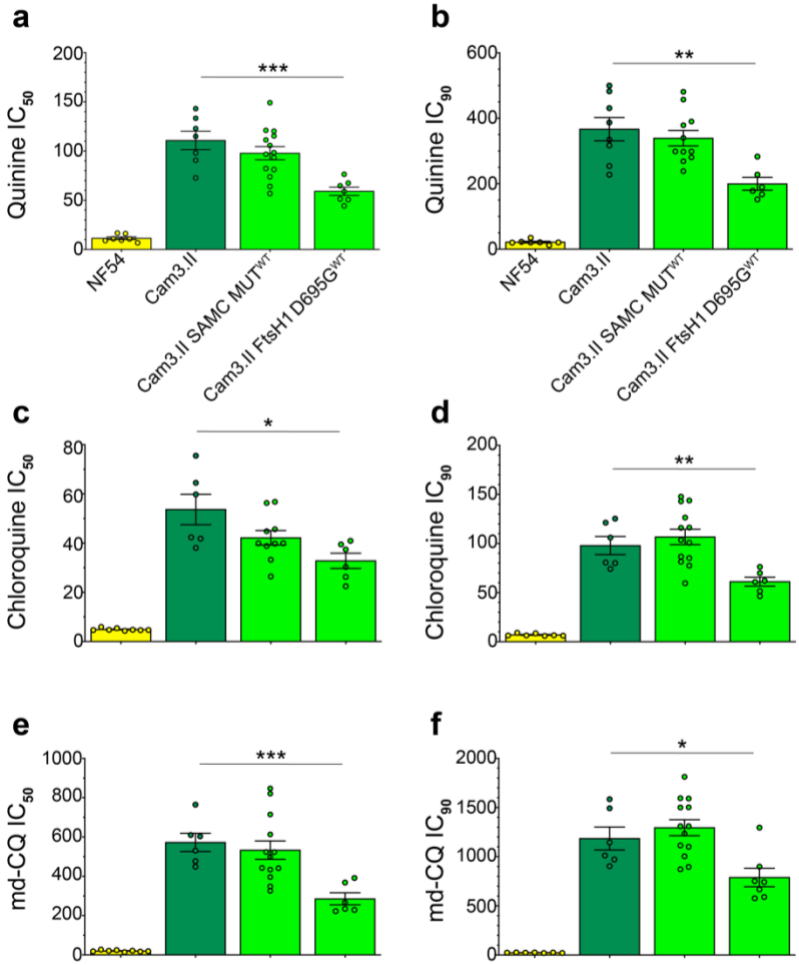

Fig. 4: *ftsh1* is a candidate gene for the chr 12 QTL locus.
a-**f**, Quinine (**a**,**b**), chloroquine (**c**,**d**), and md-Chloroquine (**e**,**f**) response in *samc* and *ftsh1* SNP-edited Cam3.II as measured by mean IC_{50} or IC_{90} values ± SEM. For each parasite, the parental unedited parasite (endogenous haplotype) (dark color) and the SNP-edited parasite (wild-type revertant parasite) (light color) were profiled. MUT, I176K/S193A. *p* values (Student's *t*-test) are indicated for the Cam3.II revertant vs the unedited Cam3.II parent (N,n=6–16,2). *$p < 0.05$; **$p < 0.01$; ***$p < 0.001$.

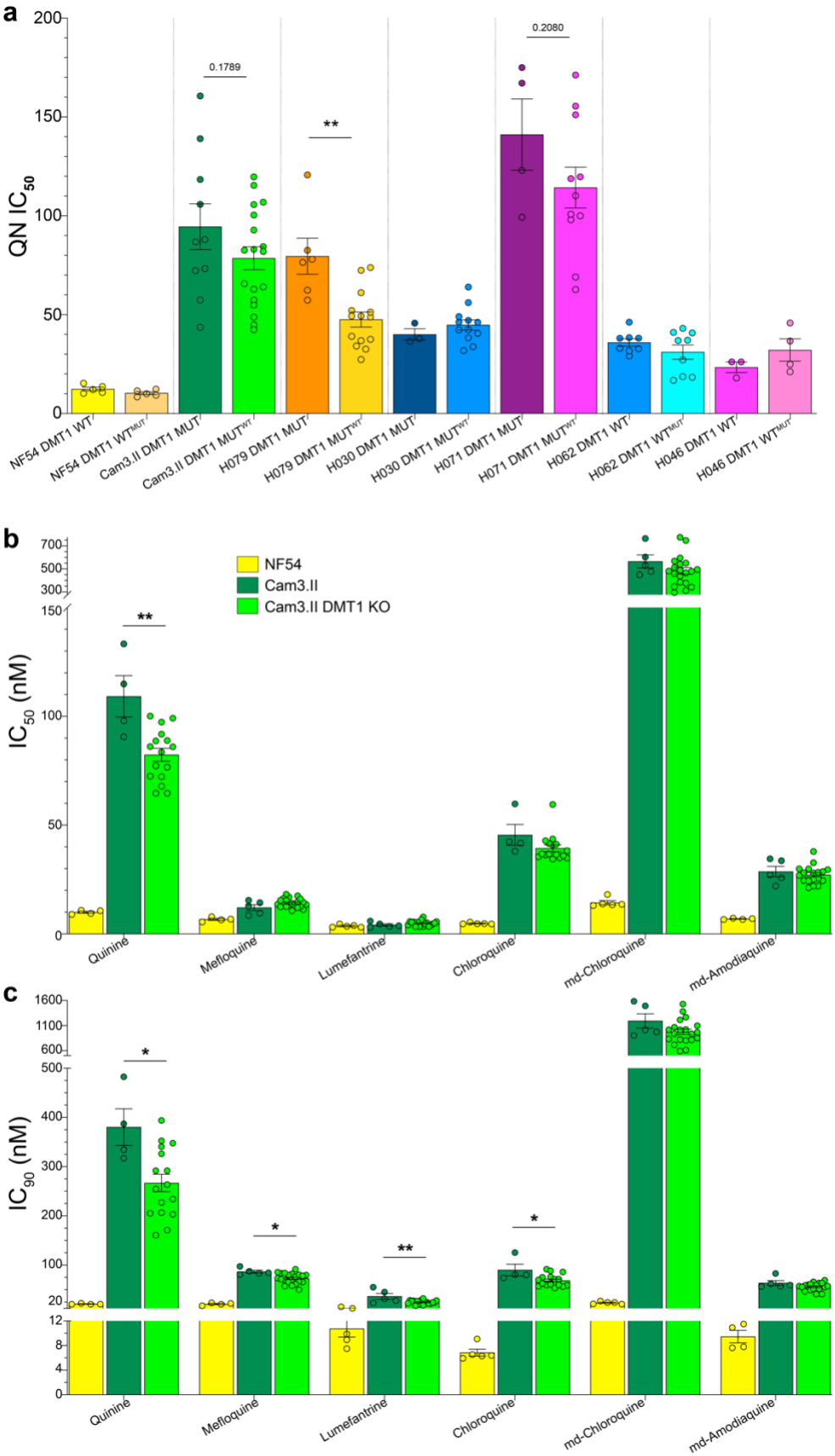

Fig. 5: DMT1 knockout significantly and specifically sensitizes Cam3.II to QN at the IC_{50} level.

a, Quinine response of DMT1 SNP-edited parents and progeny as measured by mean IC_{50} values ± SEM. For each parasite, the parental unedited parasite (endogenous DMT1 haplotype) and the SNP-edited parasite (Y107N / S129L mutant or wild-type revertant haplotype) are indicated by dark color and light color, respectively. *p* values (Student's *t*-test) are indicated (N,n=2–8,2), $^{**}p < 0.01$. WT, wild-type; YNSL, Y107N / S129L mutation. **b**,**c**, Quinine, mefloquine, lumefantrine, chloroquine, md-Chloroquine, md-Amodiaquine response in Cam3.II DMT1 knockout parasites as measured by mean IC_{50} (**a**) and IC_{90} (**b**) values ± SEM. *p* values (Student's *t*-test) are indicated for the NF54 or the KO strains vs the Cam3.II parent (N,n=4–21,2). $^{*}p < 0.05$; $^{**}p < 0.01$.

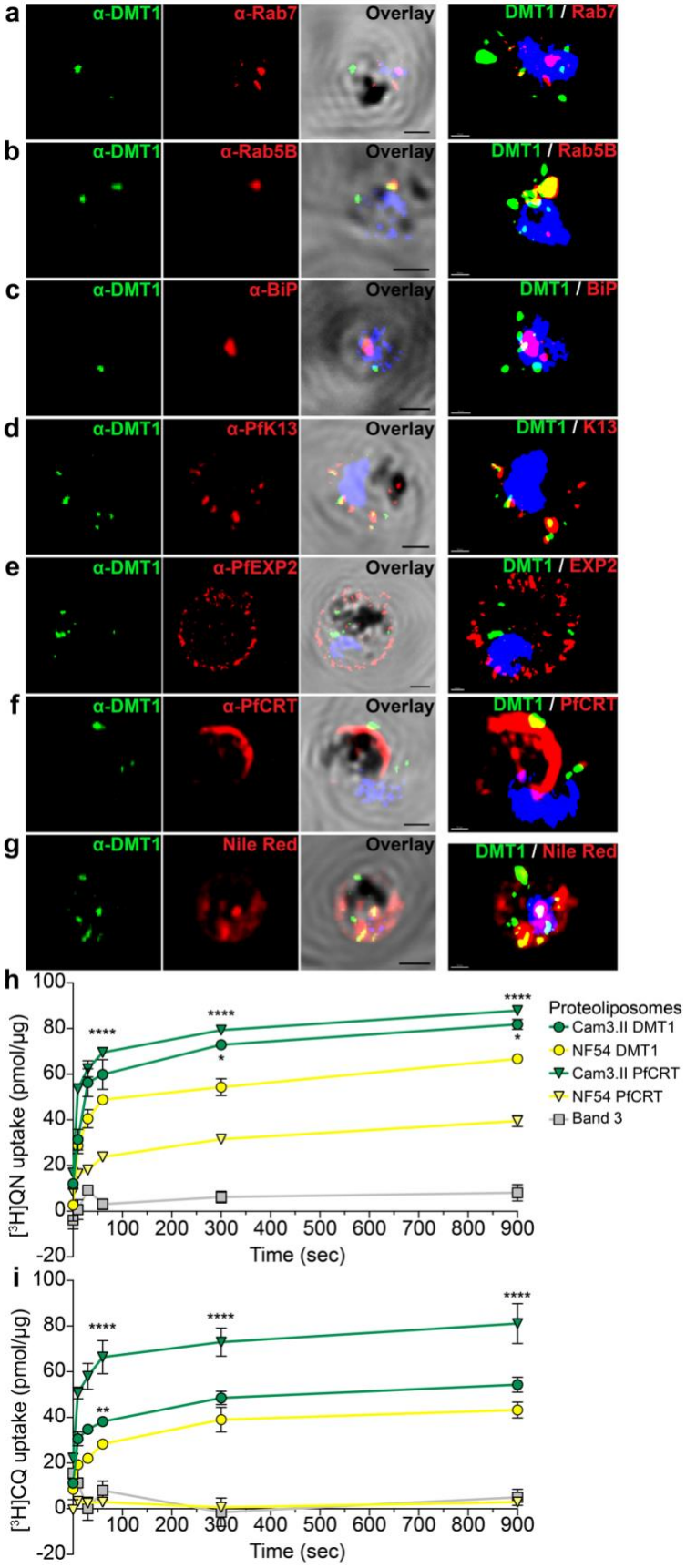

Fig. 6: DMT1 shows localization to structures associated with vesicular trafficking as well as the digestive vacuole and exhibits differential uptake of [^{3}H]QN between NF54 and Cam3.II variants.

a-**g**, Representative immunofluorescence assays (IFA) showing DMT1-3×HA-tagged parasites stained with α-HA (DMT1, green), DAPI (nuclear, blue), α-Rab7 (late endosome) (**a**), α-Rab5B (early endosome) (**b**), α-BiP (ER) (**c**), α-PfK13 (ER, vesicles, near cytostome) (**d**), α-PfEXP2 (parasitophorous vacuolar membrane) (**e**), α-PfCRT (digestive vacuole membrane) (**f**), or Nile Red (lipid bodies) (**g**) antibodies, and the 3D volume reconstructions of IFA images. Scale bars: 1 μm for IFA (black), 0.5 μm for 3D volume reconstructions (white). **h**,**i**, Time course of 300 nM [^{3}H]QN and 300 nM [^{3}H]CQ uptake measured with PfCRT (NF54 or Cam3.II), DMT1 (NF54 or Cam3.II), or Band 3-containing proteoliposomes. Data are mean ± SEM of n = 3 independent experiments performed as technical duplicates. Statistical significance between NF54 and Cam3.II variants for each protein was determined by unpaired Student's t-tests corrected for multiple testing (**h**, **i**). *p < 0.05, **p < 0.01, ****p < 0.0001.